

Soluble salts at the Phoenix Lander site, Mars: A reanalysis of the Wet Chemistry Laboratory data

J.D. Toner^{a,*}, D.C. Catling^a, B. Light^b

^a University of Washington, Dept. Earth & Space Sciences/Astrobiology Program, Box 351310, Seattle, WA 98195, USA

^b Polar Science Center, Applied Physics Laboratory, University of Washington, Seattle, WA, USA

Received 9 May 2013; accepted in revised form 24 March 2014; Available online 3 April 2014

Abstract

The Wet Chemistry Laboratory (WCL) on the Phoenix Mars Scout Lander analyzed soils for soluble ions and found Ca^{2+} , Mg^{2+} , Na^+ , K^+ , Cl^- , SO_4^{2-} , and ClO_4^- . The salts that gave rise to these ions can be inferred using aqueous equilibrium models; however, model predictions are sensitive to the initial solution composition. This is problematic because the WCL data is noisy and many different ion compositions are possible within error bounds. To better characterize ion concentrations, we reanalyzed WCL data using improvements to original analyses, including Kalman optimal smoothing and ion-pair corrections. Our results for Rosy Red are generally consistent with previous analyses, except that Ca^{2+} and Cl^- concentrations are lower. In contrast, ion concentrations in Sorceress 1 and Sorceress 2 are significantly different from previous analyses. Using the more robust Rosy Red WCL analysis, we applied equilibrium models to determine salt compositions within the error bounds of the reduced data. Modeling with FREZCHEM predicts that WCL solutions evolve Ca–Mg– ClO_4 -rich compositions at low temperatures. These unusual compositions are likely influenced by limitations in the experimental data used to parameterize FREZCHEM. As an alternative method to evaluate salt assemblages, we employed a chemical divide model based on the eutectic temperatures of salts. Our chemical divide model predicts that the most probable salts in order of mass abundance are $\text{MgSO}_4 \cdot 11\text{H}_2\text{O}$ (meridianiite), $\text{MgCO}_3 \cdot n\text{H}_2\text{O}$, $\text{Mg}(\text{ClO}_4)_2 \cdot 6\text{H}_2\text{O}$, $\text{NaClO}_4 \cdot 2\text{H}_2\text{O}$, KClO_4 , $\text{NaCl} \cdot 2\text{H}_2\text{O}$ (hydrohalite), and CaCO_3 (calcite). If ClO_3^- is included in the chemical divide model, then NaClO_3 precipitates instead of $\text{NaClO}_4 \cdot 2\text{H}_2\text{O}$ and $\text{Mg}(\text{ClO}_3)_2 \cdot 6\text{H}_2\text{O}$ precipitates in addition to $\text{Mg}(\text{ClO}_4)_2 \cdot 6\text{H}_2\text{O}$. These salt assemblages imply that at least 1.3 wt.% H_2O is bound in the soil, noting that we cannot account for water in hydrated insoluble salts or deliquescent brines. All WCL solutions within error bounds precipitate $\text{Mg}(\text{ClO}_4)_2 \cdot 6\text{H}_2\text{O}$ and/or $\text{Mg}(\text{ClO}_3)_2 \cdot 6\text{H}_2\text{O}$ salts. These salts have low eutectic temperatures and are highly hygroscopic, which suggests that brines will be stable in soils for much of the Martian summer. © 2014 Elsevier Ltd. All rights reserved.

1. INTRODUCTION

Soluble salts on Mars readily interact with water and have wide-ranging implications for aqueous processes (Squyres et al., 2004; Haskin et al., 2005). A significant motivation for the exploration of Mars is the possibility that Mars harbored life early in its history or may have life

in the subsurface today (Beatty et al., 2005). Because life requires liquid water (Tosca et al., 2008; Davila et al., 2010), the search for life has focused on aqueous alteration minerals, such as salts, which are indirect tracers of liquid water (Boynton et al., 2009; Niles et al., 2013). Salts also have key properties that can stabilize liquid water in the cold and dry conditions of Mars, such as freezing-point depression (Brass, 1980; Kuz'min and Zabalueva, 1998; Squyres et al., 2004; Bibring et al., 2006; Fairén et al., 2009; Marion et al., 2010), slower evaporation rates due to reduced water activity (Sears and Chittenden, 2005;

* Corresponding author. Tel.: +1 267 604 3488.
E-mail address: toner2@uw.edu (J.D. Toner).

Altheide et al., 2009; Chevrier et al., 2009), and hygroscopicity (Zorzano et al., 2009; Davila et al., 2010; Gough et al., 2011). In addition, cryogenic salts can incorporate water and CO₂ into their crystal structure, which will influence water and CO₂ cycling between the Martian regolith and atmosphere (Clark, 1978; Kahn, 1985; Niles et al., 2013).

The quantitative identification of salts on Mars is the first step towards determining their origin and what they mean for the evolution and habitability of Mars. Both orbital spectra and *in situ* measurements have identified salts. Key salts detected from orbit include chlorides (Glotch et al., 2008; Osterloo et al., 2008, 2010; Ruesch et al., 2012), sulfates (Gendrin et al., 2004; Langevin et al., 2005; Murchie et al., 2009), and carbonates (Bandfield et al., 2003; Ehlmann et al., 2008; Niles et al., 2013). The Mars Exploration Rovers (MERs) detected Mg, Ca, and Fe sulfates (Squyres et al., 2006; Wang et al., 2006), indicative of past acidic conditions (Hurowitz et al., 2006), and also carbonates (Morris et al., 2010), characteristic of alkaline environments. Comparisons of elemental abundance measured by landers and rovers have led to the suggestion that the soil comprises a global unit, which is a mixture of weathered and unweathered basalt, salt, dust, and meteoritic material (Clark et al., 1982; McSween and Keil, 2000; Nelson et al., 2005; Yen et al., 2005). Hence, salt compositions measured in any one locality may have global implications for the evolution and habitability of Mars.

The first direct measurements of soluble salts on Mars were made by the Wet Chemistry Laboratory (WCL) experiment on the Phoenix Lander (Boynton et al., 2009; Hecht et al., 2009; Kounaves et al., 2010a). Soluble salts were measured by adding dry soil to liquid water heated to a temperature between 5 and 10 °C, and analyzing the dissolved ions using an array of Ion Selective Electrodes (ISEs) (Kounaves et al., 2010a). The WCL experiment identified an alkaline soil solution consistent with previous pH inferences of 7.4–8.7 for soils in the Viking Lander biology experiments (Quinn and Orenberg, 1993). Phoenix also found some soluble sulfate (~1–2 wt.%), which can be compared to 5–9 wt.% total sulfate in typical soil inferred from previous landers (Kounaves et al., 2010b). This suggests that most of the soil sulfate resides in insoluble or sparingly soluble forms. One of the most interesting findings of the WCL experiment is that most of the soluble chloride is present as perchlorate (ClO₄⁻) (Hecht et al., 2009; Kounaves et al., 2010a). Perchlorates are among the most hygroscopic salts (Besley and Bottomley, 1969; Gough et al., 2011) and have eutectic temperatures as low as -75 °C (Dobrynina et al., 1980; Pestova et al., 2005), which could stabilize liquid water on present-day Mars (Marion et al., 2010).

To determine both the soluble ion chemistry and solid salt precipitates on Mars, thermodynamic models have been used, such as FREZCHEM (Marion et al., 2003, 2009, 2010, 2011). FREZCHEM suggests that a variety of parent salts are present at the Phoenix site, including calcite (CaCO₃), gypsum (CaSO₄·2H₂O), meridianiite (MgSO₄·11H₂O), NaClO₄·2H₂O, KClO₄, and Mg(ClO₄)₂·6H₂O, and that a small fraction of liquid water is stable down to about -60 °C as Mg–ClO₄-rich brine (Marion et al., 2010). However, equilibrium model predictions are sensitive to

the initial WCL chemistry that is input into the model. This deserves further attention because the Phoenix WCL analysis is characterized by relative errors in concentration between about 20–50% due to high levels of noise and anomalous signal fluctuations (Hecht et al., 2009; Kounaves et al., 2010a,b; Quinn et al., 2011). As a result, many different solution compositions are possible within error bounds.

To better understand the soluble chemistry at the Phoenix site, we reanalyzed data from the WCL experiment using improvements to the original analyses of Hecht et al. (2009) and Kounaves et al. (2010a,b) that include Kalman optimal smoothing, corrections for ion-pairs, and corrections for calibrant salts. It is important that an independent reanalysis is done because the WCL results are the only direct measurements we have of the soluble soil chemistry on Mars. With our revised ion concentrations and uncertainty estimates for the WCL aqueous solution, we apply the geochemical model FREZCHEM and a chemical divide model to determine probable parent salt compositions in the Phoenix soil, i.e. the original salt precipitates in the soil that dissolved to form the WCL solution.

2. OVERVIEW OF THE WCL EXPERIMENT

The operation and construction of the WCL experiment has been described in detail (Kounaves et al., 2009), as well as methods used to analyze the WCL data (Hecht et al., 2009; Kounaves et al., 2010a,b; Quinn et al., 2011). Briefly, the WCL instrument consists of four 40 ml beakers (labeled cells 0 to 3), each containing an array of Ion Selective Electrodes (ISEs) and other sensors for the analysis of Ca²⁺, Mg²⁺, Ba²⁺, Na⁺, K⁺, NH₄⁺, H⁺ (pH), Cl⁻, ClO₄⁻, Br⁻, I⁻, conductivity, cyclic voltammetry, anodic stripping voltammetry, and chronopotentiometry. There are three ISE sensors for measuring pH (pH_a, pH_b, and pH_{irid}). Above each WCL beaker is a 36 ml tank containing 25 ml of leaching solution with the following dissolved ions: Ca²⁺ = Mg²⁺ = Ba²⁺ = Na⁺ = K⁺ = NH₄⁺ = HCO₃⁻ = 10 μM, Cl⁻ = 50 μM, Li⁺ = 1 mM, and NO₃⁻ = 1.03 mM. During operation, the leaching solution was thawed and ejected into the WCL beaker, which is stirred by an impeller. Following this, a crucible containing salts for calibration of the ISEs was deposited into the leaching solution, bringing the solution to the composition: Ca²⁺ = 42 μM, Mg²⁺ = 34.7 μM, Ba²⁺ = 38 μM, Na⁺ = K⁺ = NH₄⁺ = HCO₃⁻ = 34 μM, Cl⁻ = 190 μM, Li⁺ = 1 mM, and NO₃⁻ = 1.1 mM. After analysis of the calibration solution, ~1 cm³ of soil sample was deposited into the WCL beaker and the sensor array was monitored over several hours. Once this initial analysis phase was finished, the heater shut down and the soil-solution was allowed to freeze in the WCL beaker. A second major phase of the WCL analyses began by thawing the frozen soil-solution in the WCL beaker. To this thawed soil-solution was added 4 mg of 2-nitrobenzoic acid to test for pH buffering in the soil, followed by three crucibles containing 0.1 g of BaCl₂ for titrimetric determination of soil SO₄²⁻. For some cells, additional thawing/freezing, soil sample addition, and sample analysis cycles were performed.

To provide context for this paper, an overview of key WCL events during the Phoenix mission operations is

shown in Table 1. Three soils were analyzed, named Rosy Red, Sorceress 1, and Sorceress 2, respectively. With respect to Sorceress 1, it is believed that acid was added on the first sol of analysis (sol 41), just after the addition of calibration salts and before sample addition, although the cause for this departure from the nominal WCL experiment is unknown (Kounaves, *personal comm.*). Furthermore, the sample drawer for Sorceress 1 appeared to be only 70–75% full, so that less soil was added to the WCL beaker than for the other soil analyses. A fourth analysis was attempted for soil Golden Goose, but it is believed that no soil entered the WCL beaker. As a result, this WCL cell was effectively run as a control blank (Kounaves et al., 2010a). This blank analysis was fortunate, because it revealed that BaCl₂ began leaking into the WCL beakers following soil sample addition, causing Cl⁻ concentrations to increase throughout the WCL analysis. Each WCL cell was designed as single use, but additional soil samples were delivered to Rosy Red and Golden Goose. A total of eight attempted sample deliveries were made, with five of them successfully entering WCL cells.

3. METHODS

3.1. WCL analysis

We analyzed ISE potentials and temperature data from the WCL experiment in two ways. First, we determined ion

concentrations in Rosy Red, Sorceress 1, and Sorceress 2 over the discrete calibration and analysis time windows given in Kounaves et al. (2010a), with some modifications, to facilitate comparison with previous estimates of ion concentrations. The data we used to derive ion concentrations are tabulated in Appendix A. Second, we analyzed ISE potentials and temperatures in Rosy Red over sols 30, 32, 34, 66, 87, and 138. We focus on Rosy Red for this more in-depth analysis because it is the least noisy of the three WCL soil experiments and it was analyzed over the most sols. Modifications to the analysis of Kounaves et al. (2010a) are described in the following subsections.

3.1.1. Kalman Smoothing

ISE potentials measured in the WCL experiment have considerable noise, partly due to a software error that caused the Oxidation Reduction Potential (ORP) electrode to switch from ground to a 650 mV source whenever pressure or temperature measurements were made. Previously, noise in the WCL data had been reduced using Fourier filtering to remove high frequencies (Kounaves et al., 2010a). We use Kalman smoothing instead because (1) Kalman smoothing does not exclude data, unlike a Fourier analysis that removes data at an arbitrary high frequency, (2) Kalman smoothing outputs an uncertainty estimate of the signal, and (3) it can be shown that the Kalman filter is mathematically the best linear filter for dealing with noisy data where one can assume uncorrelated noise (Simon,

Table 1

Overview of WCL activities in the Phoenix mission, compiled from tables in Kounaves et al. (2010a) and Arvidson et al. (2009).

Sol	Cell	WCL Experiment Activity
25	0	Rosy Red (#1) – surface sample collected down to ~2.5 cm depth from polygon center in the Burn Alive trench
30 ^a	0	Rosy Red (#1) – ISE calibration and sample delivery
32 ^a	0	Cell thawed
34 ^a	0	Acid and three BaCl ₂ crucibles added
34 ^a	1	Sorceress 1 – sublimation lag sample collected from a soil scraped off of subsurface ice at ~3 cm depth in the Snow White trench, in a polygon center
41 ^a	1	Sorceress 1 – ISE calibration, acid addition, and sample delivery. Note: the sample delivery drawer appeared to be only 70–75% full
43 ^a	1	Three BaCl ₂ crucibles added. Note: acid appears to have been added on sol 41
66 ^a	0	Rosy Red (#2) – surface sample collected down to ~2.5 cm depth from the Rosy Red 2 trench, adjacent to the Burn Alive trench. Sample redelivery
78 ^a	0	Thermal diagnostic run
87 ^a	0	Open loop diagnostic run
95	3	Golden Goose – subsurface sample collected from the Stone Soup trench
96 ^a	3	Golden Goose – attempted sample delivery, unsuccessful
101	3	Golden Goose – subsurface sample collected from same location in the Stone Soup trench
102 ^a	3	Golden Goose – attempted sample redelivery, unsuccessful
105	2	Sorceress 2 – sublimation lag sample collected from a soil scraped off of subsurface ice at ~3 cm depth in the Snow White trench, in a polygon center
107 ^a	2	Sorceress 2 – ISE calibration and sample delivery
116 ^a	2	Acid and 1st BaCl ₂ crucibles added
127 ^a	2	2nd BaCl ₂ crucible added
131 ^a	2	Cell thawed
134 ^a	2	3rd BaCl ₂ crucible added
136	0	Rosy Red (#3) – surface sample collected down to ~2.5 cm depth from the Rosy Red 3 trench, adjacent to the Burn Alive trench
138 ^a	0	Rosy Red (#3) – attempted sample redelivery, unsuccessful
147 ^a	3	Golden Goose – attempted sample push, unsuccessful

^a Sols during which ISE potentials and beaker temperatures were monitored.

2006, Chapter 5). An extensive literature describes the Kalman filter (Simon, 2006), and its use in analytical chemistry is reviewed in a number of papers (e.g. Brown, 1986; Lavagnini et al., 1990; Rutan, 1991).

For a simple system that varies randomly with associated noise, known as a local level model, the Kalman filter describes the state of the system (x_t) at time t as $x_t = x_{t-1} + \epsilon$ and measurements (y_t) made on the system as $y_t = x_t + \eta$, where ϵ is the process noise and η is the measurement noise. The process and measurement noise are assumed to be independent and normally distributed with respective covariances. Kalman smoothing recursively estimates the true state of the system x_t from measurements y_t by giving less weight to individual noisy measurements. To implement Kalman smoothing, we use the KFAS package available in the statistical program R (Helske, 2010; Tusell, 2011). KFAS accounts for missing data points in a time series, which are common in the WCL data, and estimates the variance of the process and measurement noise using a maximum likelihood method (function fitSSM in KFAS).

We applied Kalman smoothing to the raw temperature data and minimally processed ISE potential data. Prior to smoothing the ISE potentials, we referenced the ISE potentials to one of two Li^+ ISEs and removed spurious ISE potentials measured within one second preceding a temperature/pressure measurement, as in Kounaves et al. (2010a). We then removed obvious outliers. For the analysis of the WCL data over discrete time windows, we estimated the noise characteristics of the temperature and ISE potentials over the duration of each discrete time window (exact time windows are specified in Appendix A). We then applied Kalman smoothing, which computes both the smoothed signal and error estimates, the latter based on the noise level in the data. Because smoothed temperatures and ISE potentials vary over these time intervals, the values we use for calculating ion concentrations are the average values over the time intervals. Uncertainties in these average values are derived by adding in quadrature the uncertainty in the smoothed values over the time interval and the average estimated uncertainty in the smoothed values output by KFAS. For the time-varying analysis of Rosy Red, we estimated the time-varying process and measurement noise in the temperature and ISE potential data over five minute time windows. We then applied Kalman smoothing using the time-varying noise characteristics.

3.1.2. Reanalysis of ISE calibration slopes

Initially, it was thought that the ISE sensors could be calibrated with a two-point *in situ* calibration using ISE potentials measured in the leaching solution and the calibration solution (Kounaves et al., 2009); however, later sensitivity analyses indicated that this method of calibration would introduce large errors into the analysis because the concentrations in the two dilute solutions occupy only a small part of the dynamic range (Grunthaner et al., 2009). It was determined that the best calibration method is a one-point calibration using ISE potentials measured in the calibration solution and ISE slopes previously determined during five Earth-based calibrations. In our data reduction, we find that the errors associated with the

Earth-based calibration slopes have the largest influence on final concentration errors. Although five Earth-based calibrations were performed, we exclude the JPL functional test calibration from our calculations, as did Kounaves et al. (2010a), because the JPL functional test slopes are consistently lower than in the other four calibrations.

To better characterize uncertainties in the Earth-based calibration slopes, we applied least squares linear fits to ISE potential vs. log activity data measured in the four Earth-based calibrations (Grunthaner et al., 2009). We then calculated final ISE calibration slopes as the weighted mean of the Earth-based calibration slopes, using the error in the linear fits as the weights (Table 2). Errors in the final calibration slopes are calculated as the unbiased standard deviation of the weighted mean. The pH sensor slopes are derived from pre-flight calibrations that used two test solutions saturated with 5% CO_2 (Grunthaner et al., 2009). Errors in the pH sensor slopes are determined by propagating errors in the two individual pH ISE measurements to the slope. The calibration slope for the ClO_4^- ISE sensor was measured on a spare flight beaker at a temperature of 7 °C (Kounaves et al., 2010a). We assume that the error in the ClO_4^- ISE sensor slope is 0.7 mV dec^{-1} , near the average error for the other ISE sensors.

3.1.3. Ionic strength

The conductivity sensor, used for measuring ionic strength, failed during the Rosy Red analysis. We calculate the ionic strength of Rosy Red by calculating an initial ionic strength, accounting for ions already present in the calibration solution, and iteratively refine this value by using the resulting concentrations to calculate a new ionic strength until convergence. The ionic strength we use is the effective ionic strength, which accounts for ion pairs in solution. For Sorceress 1 and Sorceress 2, we use ionic strength values determined from conductivity measurements in Kounaves et al. (2010a).

3.1.4. Debye–Hückel model

To determine activity coefficients from ionic strength, we used the temperature dependent Debye–Hückel ion-association model. For a given ion i with hydrated radius a_i and charge z_i , the Debye–Hückel activity coefficient γ_i is given by:

$$\log \gamma_i = \frac{-Az_i^2\sqrt{I}}{1 + Ba_i\sqrt{I}} \quad (1)$$

with temperature dependent parameters A and B. We incorporated this temperature dependence into our WCL data reduction using the empirical equations:

$$A = 1.824928 \times 10^6 \rho_0^{1/2} (\epsilon T)^{-3/2} \quad (2)$$

$$B = 50.3 (\epsilon T)^{-1/2} \quad (3)$$

where ϵ is the dielectric constant of water, T is temperature in Kelvin, and ρ_0 is the density of water (Langmuir, 1997). The temperature dependence of ϵ is given by:

$$\epsilon = 2727.586 + 0.6224107T - 466.9151 \ln T - 52000.87/T \quad (4)$$

Table 2

ISE slopes (mV dec^{-1}) calculated from four Earth-based calibrations with $\pm 1\sigma$ error. The JPL functional test calibration was excluded because it was consistently different from the four other calibrations performed. All calibrations were performed at ‘room temperature’ (the precise temperature was not recorded, but we assume a value of 22°C), except for the ClO_4^- sensor, which was calibrated at 7°C .

	Rosy Red – flight unit 20	Sorceress 1 – flight unit 18	Sorceress 2 – flight unit 22
pH_a	55.97 ± 0.46	59.35 ± 0.40	58.11 ± 0.34
pH_b	57.23 ± 0.44	59.77 ± 0.43	55.79 ± 0.30
pH_{irid}	52.40 ± 0.39	56.43 ± 0.33	52.40 ± 0.42
Mg	28.68 ± 0.65	28.12 ± 0.75	29.09 ± 0.47
Ca	29.13 ± 0.84	28.86 ± 0.58	29.06 ± 0.28
K	59.01 ± 0.60	59.07 ± 1.50	58.96 ± 0.38
Na	53.54 ± 0.97	52.89 ± 0.45	53.70 ± 1.12
NH_4	59.59 ± 0.74	59.23 ± 1.05	59.77 ± 0.80
Cl	-54.91 ± 0.29	-54.34 ± 0.23	-53.98 ± 0.31
ClO_4^a	-62.00 ± 0.70	-62.00 ± 0.70	-62.00 ± 0.70

^a The ClO_4^- sensor was calibrated only once, so the error is assumed.

3.1.5. Ion-pair corrections

The WCL ISE sensors measure the activity of unpaired ions, but MgSO_4^0 and CaSO_4^0 ion-pairs can be significant in solution (Kounaves et al., 2010b), resulting in an underestimation of Mg^{2+} and Ca^{2+} concentrations and an overestimation of unpaired SO_4^{2-} concentrations. We corrected for ion-pairs using the phreeqc.dat database in the aqueous geochemical program PHREEQC (Parkhurst and Appelo, 1999) by adding ions until the unpaired species activity equaled that determined in the WCL analysis. The values of the ion pair concentrations are given later in Section 4.

3.1.6. Calibration/leaching solution ions

Prior to the addition of soil samples, the WCL solution contained ions from salts dissolved in a calibration solution. To correct for ion concentrations already present from the WCL calibration solution, we subtracted these ions from the final results. This simple correction, which was previously neglected, has a significant effect on low concentration ions such as Cl^- and Ca^{2+} , which is described in Section 4.

3.1.7. Calibration of the pH ISE Sensors

Kounaves et al. (2010a) calibrated pH ISE sensors using ISE potentials measured after the addition of leaching solution, but before the sample drawer had opened, at which point the pH was assumed to equal 5.1. This method could be used only for a few sensors because most of the pH ISEs had unstable signals prior to the first drawer opening. As a result, pH could not be determined for the pH_{irid} sensor in Rosy Red and Sorceress 1, and none of the Sorceress 2 pH ISE sensors could be analyzed. To obtain values from the Rosy Red and Sorceress 1 pH_{irid} sensors, we calibrated these sensors to the pH_a sensors, which can be calibrated as in Kounaves et al. (2010a). We did this by referencing the pH_{irid} sensors to the pH measured after the addition of calibration salts (specific time intervals are given in Appendix A); the Rosy Red and Sorceress 1 pH_a sensors

indicate that the pH after the addition of calibration salts was 5.3 and 3.8 respectively. For the Rosy Red pH_{irid} sensor, we used a later analysis interval than for all the other analytes. This is because the pH_{irid} sensor appears to respond more sluggishly than the pH_a sensor and is still decreasing during the analysis interval used for other ions (see graphs in Appendix B). A similar slow response does not seem to affect either the Sorceress 1 or 2 pH_{irid} sensors.

Because none of the Sorceress 2 pH ISE sensors could be calibrated as in Kounaves et al. (2010a), we calibrated these sensors by assuming that the pH after the addition of calibration salts is the same as for Rosy Red after the addition of calibration salts ($\text{pH} = 5.3$). This assumption is reasonable because the composition of the calibration salts was the same for each WCL cell and the same number of drawer opening events occurred prior to the addition of calibration salts. However, the first drawer opening for Sorceress 2 occurred an hour after the solution thawed, which may have allowed much more CO_2 to be expelled during the first drawer opening. Such a CO_2 release would have raised the pH of the calibration solution. As a result, the pH for Sorceress 2, calibrated as described above, may be a minimum value (i.e. the actual value may be somewhat higher). We note that the pH of Sorceress 1 is also a minimum pH because acid had been added to Sorceress 1 before the soil sample addition (Kounaves, *personal comm.*).

3.2. Calculating ion concentrations

Procedures for calculating ion concentrations from the WCL data are discussed in Kounaves et al. (2010a). Briefly, ion concentrations are calculated using the equation:

$$C_s = \frac{1}{\gamma} 10^{\left[\frac{E_s}{S_M} - \frac{E_C}{S_M} + \log(a_C) \right]} \quad (5)$$

where C_s (molal) is the sample ion concentration, γ is the ion activity coefficient, E_s (mV) is the potential measured after soil sample addition, E_C (mV) is the potential measured during the calibration interval, a_C is the ion activity in the calibration solutions, and S_M (mV dec^{-1}) is the temperature corrected ISE slope. ISE slopes measured at temperature T_E on Earth (S_E) are corrected for the temperature of the WCL solution on Mars (T_M) using the equation:

$$S_M = S_E \frac{T_M}{T_E} \quad (6)$$

where temperatures are in Kelvin. The Earth-based calibrations were done at ‘room temperature’, but the precise temperature was not recorded. We assume here that T_E is 22°C .

Several additional corrections are necessary to calculate NH_4^+ , ClO_4^- , and Ca^{2+} concentrations. The NH_4^+ ISE sensor is also sensitive to K^+ . This is corrected for by assuming that K^+ contributes an additional activity of $0.15a_{\text{K}^+}$ to the measured NH_4^+ activity. Because perchlorate was not expected on Mars, ClO_4^- was not included in the calibration solution. As a result, the ClO_4^- ISE sensor was calibrated to its lower activity detection limit of 10^{-6} (i.e. $a_C = 10^{-6}$ in Eq. (6)). Finally, the Ca^{2+} ISE sensor is also sensitive to

ClO_4^- ions and has a Nernstian response to ClO_4^- with a slope of -29 mV dec^{-1} . To correct the measured sample ISE potential for the bias introduced by ClO_4^- , we use the equation (Kounaves et al., 2010a):

$$E_{\text{Ca}^{2+}_{\text{corr}}} = E_{\text{Ca}^{2+}} - \frac{S}{2} [\log(a_{\text{ClO}_4^-}) - \log(9.5 \times 10^{-6})] \quad (7)$$

where $E_{\text{Ca}^{2+}_{\text{corr}}}$ is the corrected Ca^{2+} ISE potential, S is -29 mV dec^{-1} , and 9.5×10^{-6} is the lower activity limit for the ClO_4^- bias on the Ca^{2+} ISE sensor. We assume an error of 0.7 mV dec^{-1} for S .

Error propagation for any given function q (with variables x , y , etc.) is determined in quadrature using the standard error propagation equation:

$$\sigma_q^2 = \left(\frac{\partial q}{\partial x} \sigma_x \right)^2 + \left(\frac{\partial q}{\partial y} \sigma_y \right)^2 + \dots \quad (8)$$

We use symmetric errors, as opposed to the asymmetric errors used in Kounaves et al. (2010a), because the observed asymmetry in the ISE potential and temperature data is small (see Appendix B). Eq. (9) assumes that all variables are uncorrelated; however, temperatures are correlated with ISE potentials due to the temperature dependence of ISE slopes. We do not include this correlation in our error analysis because the additional error is negligible. For example, the correlation coefficient between temperature and K^+ ISE potential in Rosy Red is low, -0.05 and -0.03 for the calibration and analysis intervals respectively. Accounting for this correlation changes the final concentration errors by $<0.1\%$. Partly, the poor correlation is due to noise in the temperature and ISE potential data. Additionally, a non-Nernstian temperature response in ISE potentials may have arisen if temperature variations in the soil solution were damped relative to those in the beaker wall, within which the temperature sensor was embedded. This inference is supported by measurements as WCL beakers warm above 0°C where a plateau in temperature might be expected as ice melts endothermically, but none is seen (e.g., cell 3, sol 107, $\sim 10:30$ LMST).

4. WCL ANALYSIS RESULTS

Final concentration values resulting from our reanalysis of the Rosy Red, Sorceress 1 and 2 WCL experiments using the methods described above indicate that Phoenix soils are alkaline, rich in Mg^{2+} , Na^+ , ClO_4^- , and SO_4^{2-} , low in Ca^{2+} , Cl^- , and K^+ , and deficient in NH_4^+ (Table 3). Our analysis of Rosy Red is generally consistent with Kounaves et al. (2010a,b); however, several ions in Rosy Red are higher in concentration than in Kounaves et al. (2010a) due to the higher ionic strength we calculate (0.017 m vs. 0.008 m), and our Ca^{2+} and Cl^- concentrations are lower due to the correction for ions from the calibration salts. Ions in the Rosy Red calibration solution account for 21% of the measured Ca^{2+} and 32% of the Cl^- . By accounting for MgSO_4^0 ion-pairs in Rosy Red, the total Mg concentration increases by 20%. In contrast to Rosy Red, ion concentrations for Sorceress 1 and 2 are significantly different from values in Kounaves et al. (2010a,b), often outside of $\pm 1\sigma$. In general, ion concentrations between Rosy Red,

Sorceress 1 and 2 vary in our analysis, which suggests that soluble salt compositions in Phoenix soils are more heterogeneous than previously thought.

Soil pH values determined in our analysis are generally consistent with previous inferences of an alkaline soil (Table 3). In Rosy Red and Sorceress 1, pH values determined for previously unanalyzed pH_{irid} sensors (the method we use is described in Section 3.1.7) are somewhat different from pH values determined using the calibration method in Kounaves et al. (2010a). This may be due to problems with the pH_{irid} sensor (the pH_{irid} sensor is different from the polymer-based pH_a and pH_b sensors, and we note that the pH_{irid} sensor appears to respond sluggishly in Rosy Red); however, consistent values between all three pH sensors are obtained for Sorceress 2. The measured pH of Sorceress 2 is near 6.8, but this value may be a minimum due to the possible increase in the calibration pH from CO_2 outgassing during drawer openings. The pH of Sorceress 1 may also be a minimum because acid was added to the cell before the soil sample addition, which may have neutralized some of the sample alkalinity. Hence, the only accurate WCL pH measurement with its own internal calibration was measured by the Rosy Red pH_a ISE sensor, giving a pH of 7.7.

Differences in ion concentrations and errors between this study and Kounaves et al. (2010a,b) for Sorceress 1 and 2 are likely due to differences in the treatment of temperatures, ISE potentials, Earth-based calibration slopes, and errors. A sensitivity analysis on Rosy Red, in which Mg^{2+} concentrations are calculated by varying each measured parameter by $\pm 2\sigma$, reveals that changes in the Earth-based calibration slope have the greatest effect on calculated ion concentrations (Table 4). However, our calibration slopes are similar to Kounaves et al. (2010a) and changing them to the precise values used in Kounaves et al. (2010a) does not resolve differences in concentration values, which indicates that variations in other measured parameters are affecting the final concentrations. In Rosy Red, the noise level was relatively low and ISE potentials were stable, so that we obtained similar results regardless of our different smoothing method. In contrast, Sorceress 1 and 2 are characterized by much greater noise. As a result, the Kalman smoothing we use may have caused our analysis to differ significantly from Kounaves et al. (2010a), which used Fourier filtering to remove noise at an arbitrary, unspecified cut-off frequency.

Our analysis of errors accounts for random, uncorrelated errors, such as electronic signal noise, but we cannot account for systematic errors due to shifts in calibration or fluctuations in the ORP. Other possible sources of systematic error include the possibility that calibration salts only partially dissolved in Sorceress 1, leakage of BaCl_2 reagent into the WCL cells, ionic interferences in the ISE potentials, and uncertainties in the conductivity analysis (Kounaves et al., 2010a). Systematic errors due to BaCl_2 leakage can be evaluated by examining the change in the Cl^- ISE potential over time. Furthermore, ionic interferences have been estimated and can be accounted for, such as the influence of K^+ on the NH_4^+ ISE sensor (Lukow and Kounaves, 2005) and the bias introduced in the Ca^{2+}

Table 3

Total ion concentrations (mM) and pH in Rosy Red, Sorceress 1, and Sorceress 2 from this study and from previous analyses by Kounaves et al. (2010a,b).

	Rosy Red		Sorceress 1		Sorceress 2	
	This study	Previous	This study	Previous	This study	Previous
pH _a	7.67 ± 0.08	7.74 ^{+0.11} _{-0.11}	>7.32 ± 0.08	7.62 ^{+0.18} _{-0.12}	>6.52 ± 0.06 ^a	–
pH _b	– ^b	– ^b	>7.40 ± 0.08	7.61 ^{+0.16} _{-0.12}	>6.86 ± 0.09 ^a	–
pH _{irid}	8.30 ± 0.08 ^a	–	>7.00 ± 0.12 ^a	–	>6.80 ± 0.13 ^a	–
Ca ²⁺	0.16 ± 0.07	0.55 ^{+0.75} _{-0.34}	0.45 ± 0.18	0.42 ^{+0.76} _{-0.31}	0.09 ± 0.04	0.60 ^{+0.79} _{-0.34}
Mg ²⁺	2.91 ± 0.85	2.90 ^{+1.90} _{-1.20}	6.22 ± 2.23	2.20 ^{+2.00} _{-1.10}	1.31 ± 0.42	3.70 ^{+3.00} _{-1.70}
Na ⁺	1.46 ± 0.33	1.40 ^{+0.65} _{-0.48}	3.52 ± 0.45	1.10 ^{+0.60} _{-0.38}	0.99 ± 0.28	1.40 ^{+1.00} _{-0.61}
K ⁺	0.33 ± 0.05	0.36 ^{+0.29} _{-0.17}	0.50 ± 0.17	0.17 ^{+0.20} _{-0.10}	0.17 ± 0.03	0.39 ^{+0.32} _{-0.17}
NH ₄ ⁺	0.02 ± 0.01	0.04 ^{+0.04} _{-0.01}	-0.03 ± 0.01	–	0.00 ± 0.01	0.03 ^{+0.06} _{-0.03}
Cl ⁻	0.39 ± 0.04	0.60 ^{+0.14} _{-0.12}	0.79 ± 0.14	0.24 ^{+0.11} _{-0.13}	0.24 ± 0.03	0.47 ^{+0.21} _{-0.11}
ClO ₄ ⁻	2.89 ± 0.54	2.70 ^{+1.40} _{-0.95}	2.11 ± 0.50	2.10 ^{+0.86} _{-1.20}	2.72 ± 0.57	2.20 ^{+2.20} _{-0.81}
SO ₄ (total)	4.17 ± 3.47	4.80 ^{+1.50} _{-1.50}	– ^b	– ^b	4.97 ± 1.44	5.90 ^{+1.50} _{-1.50}
CaSO ₄ ⁰	0.05	–	– ^b	– ^b	0.02	–
MgSO ₄ ⁰	0.56	–	– ^b	– ^b	0.28	–

^a pH values calculated by calibrating to the pH_a ISE sensors as described in Section 3.1.7.

^b No value is given due to an ISE sensor failure.

Table 4

A sensitivity analysis of Mg²⁺ concentrations (mM) in Rosy Red. Values for temperature, ISE potential, ionic strength, and slope are varied from the original value by ±2σ. The difference between the -2σ and +2σ values, Δ2σ, is shown in the far right column.

Measurement	-2σ	Original	+2σ	Δ2σ
Calibration temperature	2.92	2.91	2.81	0.11
Calibration ISE potential	3.11	2.91	2.64	0.47
Calibration slope	3.87	2.91	2.21	1.66
Analysis temperature	2.83	2.91	2.90	-0.07
Analysis ISE potential	2.54	2.91	3.23	-0.69
Ionic strength	2.50	2.91	3.11	-0.61

ISE potential by ClO₄⁻ (Kounaves et al., 2010a). Systematic errors due to fluctuations in the ORP appear to be pervasive throughout the WCL analyses. With respect to Rosy Red, the signal on sol 30 behaves largely as expected for a nominal WCL experiment and appears to be minimally affected by the ORP (Fig. 1A). In contrast, Sorceress 1 and 2 on sols 41 and 107 respectively are characterized by large and anomalous signal fluctuations before the addition of calibration salts and after the soil analysis (Kounaves et al., 2010a). Quantifying systematic errors in these analyses would be difficult, but would increase the errors for ion concentrations in Sorceress 1 and 2.

Unfortunately, systematic errors due to shifts in the calibration are difficult to detect because a two-point calibration of the right dynamic range could not be performed repeatedly on Mars, but the method of calibration using the Earth-based calibration slope is expected to cause an additional relative error of only 2–4% in ion activity for concentrations similar to the WCL solutions (Grunthaner et al., 2009). This is small compared to the errors in Table 3. However, it is likely that errors in the pH ISE slopes are underestimated. This is because the pH ISE slopes were determined using only a single two-point calibration and the measured WCL pH values are beyond the calibration range (the two calibration pHs were near 5.0 and 6.7). If repeated, more complete calibrations had been done, we

could be more confident of the pH ISE slopes and the estimated error in the pH ISE calibration slopes would probably be larger; however, even if the calibration slope of the Rosy Red Ph_a sensor is varied by ±5 mV dec⁻¹, the calculated pH varies only by approximately ±0.25. The pH values are not used in any of the modeling later in this paper, so they do not affect our conclusions.

We extended our analysis of Rosy Red by analyzing ISE potentials and temperatures over sols 30, 32, 34, 66, 87, and 138 (Fig. 2). During sol 30, ISE potentials change sharply upon addition of calibration salts and sample, and attain relatively constant values at other times. Ion concentrations calculated from potentials after the addition of sample remain within error bounds of the values in Table 3, with the exception of Cl⁻, due to leakage of BaCl₂ reagent, and the pH. The Cl⁻ ISE appears to be affected by the BaCl₂ leakage only after the addition of soil sample, which suggests that the soil analysis was minimally affected by BaCl₂ leakage. The concentration of Cl⁻ at the end of sol 30 is 3.9 mM, indicating that 3.5 mM of Cl⁻ had leaked into the WCL cell by the end of sol 30. Assuming that this Cl⁻ was from the BaCl₂ leak, this corresponds to 9.1 mg of BaCl₂ or 3% of the total BaCl₂ in all three crucibles (0.3 g BaCl₂ total). The pH_a ISE increases slowly after the addition of soil, from a value of -16.6 mV during the analysis window to a value to 18 mV at the end of sol 30. For a temperature corrected ISE slope of 53.4 mV dec⁻¹, this indicates a decrease in the pH by 0.65 over a period of five hours. Such slow drifts in pH are common in measurements of soil pH and downward drifts in pH have been noted to occur in oxide-rich soils after addition of base due to the buffering capacity of OH groups on oxide surfaces, which gradually desorb protons (Onoda and De Bruyn, 1966). Alternatively, Quinn et al. (2011) suggested that the BaCl₂ leak caused the slow decrease in pH. The addition of BaCl₂ to the WCL solution should precipitate insoluble BaCO₃, which would decrease the solution alkalinity and lower the pH. However, using PHREEQC, we model a pH decrease of only ~0.01 in Rosy Red due to BaCl₂ leakage,

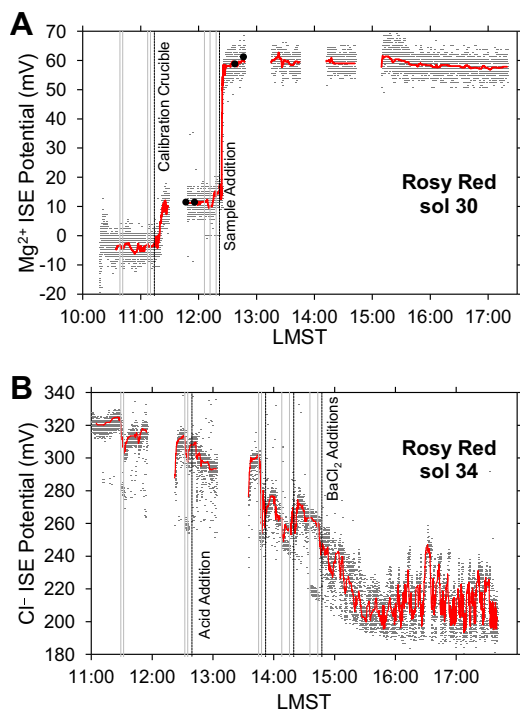


Fig. 1. Examples of relatively clean and noisy ISE data from the Rosy Red analysis. Gray data points are ISE potentials referenced to a Li^+ ISE, and red lines are Kalman smoothed values. Drawer opening events are indicated by gray dashed vertical lines, and other major events are indicated by black dashed vertical lines. Additional graphs juxtaposing raw and Kalman smoothed data on sol 30 are presented in Appendix B. (A) Mg^{2+} ISE potentials on sol 30. The calibration and sample analysis intervals are indicated by black dots. (B) Cl^- ISE potentials on sol 34 showing data affected by ORP fluctuations. The increase in the Ba^{2+} ISE potential used to flag the endpoint of the SO_4^{2-} titration occurred upon addition of the second BaCl_2 crucible. (For interpretation of the references to colour in this figure legend, the reader is referred to the web version of this article.)

far less than the observed 0.65 pH decrease. In our modeling, we assume that 1.75 mM BaCl_2 had leaked into the WCL cell (based on the observed Cl^- increase over sol 30), a pCO_2 of ~ 4 mbar, and an alkalinity of 2 mM, adjusting SO_4^{2-} for charge balance. The observed pH decrease of 0.65 can be replicated in PHREEQC only if ~ 50 times more BaCl_2 had leaked into the cell, which suggests that the pH decrease was not caused by the BaCl_2 leak.

After sol 30, ISE potentials have large and anomalous variations from sol to sol (Fig. 2). We speculate that the large offsets in ISE potentials over successive sols are due to changes in the ISE calibration induced by repeated freeze–thaw cycles in the WCL beaker (see Fig. 2, lower panel). Changes in ISE calibration upon freeze/thaw cycles imply that absolute ion concentrations cannot be accurately determined after the initial sol of analysis. For most ions, ISE potentials increase following the previous sol. In particular, the Cl^- ISE potential is higher during sol 32 and the beginning of sol 34 than at the end of sol 30, perhaps sug-

gesting that Cl^- had decreased in concentration (note: there is an inverse relationship between potential and concentration for anions). Near the rapid increase in Ba^{2+} upon addition of the second BaCl_2 crucible, indicated by the spike in Ba^{2+} ISE potential, the Cl^- ISE potential is used to infer the SO_4^{2-} content of Rosy Red (Kounaves et al., 2010b); however, the Cl^- ISE potential at this point is similar to its value at the end of sol 30. Furthermore, ISE potentials on sol 34 appear to be adversely affected by fluctuations in the ORP, more so than on other sols (Fig. 2 and Fig. 1B). These observations indicate that Cl^- ISE potentials used to calculate SO_4^{2-} concentrations are inaccurate. To account for additional errors in the SO_4^{2-} measurements in Rosy Red due to systematic errors in the Cl^- ISE potentials on sol 34, we add an additional error of ± 15 mV to the Cl^- ISE potential on sol 34. We base this additional systematic error on the uncertainty in the Cl^- ISE potential near the end of sol 34, keeping in mind that there may be additional error because of shifts in the calibration. No additional error is added to the SO_4^{2-} analysis in Sorceress 2.

The accuracy of aqueous chemical analyses is commonly checked by calculating the charge balance; a charge balance near zero indicates that all major species have been accurately accounted for. The charge balances of Rosy Red, Sorceress 1 and 2 are -12.7% , 71.8% , and -53.1% respectively. For reference, charge balances in Earth-based aqueous analyses are typically less than $\pm 10\%$, and a charge balance less than $\pm 5\%$ is considered a good aqueous analysis (Fritz, 1994). Sorceress 1 has a positive charge balance, indicating that there is a large anion deficiency in the analysis. This makes sense because SO_4^{2-} , a significant component in Rosy Red and Sorceress 2, could not be analyzed in Sorceress 1 due to a failure of the Ba^{2+} ISE (Kounaves et al., 2010b). Charge balances for both Rosy Red and Sorceress 2 are negative, indicating either excess anions in the analysis or that cation concentrations are deficient. The presence of another major cation besides Ca^{2+} , Mg^{2+} , Na^+ , or K^+ is unlikely because these ions account for nearly all of the positive charge in most natural waters. Furthermore, Quinn et al. (2011) concluded that Fe^{2+} and other redox active species are not present in significant concentrations based on oxidation–reduction potential measurements. Ferric sulfates ($\text{Fe}_2(\text{SO}_4)_3$) have been found on Mars (Johnson et al., 2007; Lane et al., 2008) and may contribute Fe^{3+} to solution; however, substantial Fe^{3+} is only soluble in acidic waters, which is inconsistent with the alkaline pH of Phoenix soils. Given that all major cations in the WCL solutions were probably measured, the negative charge balance in Rosy Red and Sorceress 1 suggests that either Cl^- , ClO_4^- , or SO_4^{2-} concentrations were overestimated in the WCL analyses, especially considering that unanalyzed anions were probably present in the WCL solutions, as discussed in the following paragraph. We suggest that SO_4^{2-} concentrations are overestimated because the SO_4^{2-} concentrations are either close to or exceed the total cation charge and the SO_4^{2-} analysis is subject to the most error.

Although it is unlikely that another major cation is present in the WCL solutions, it is likely that some anions were

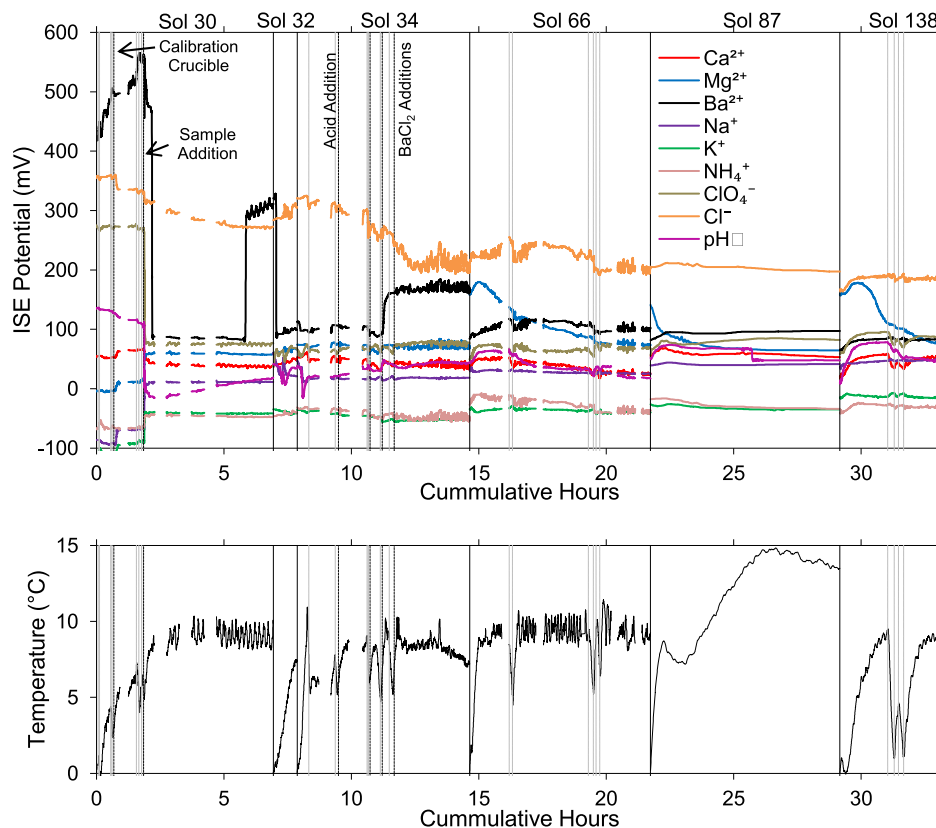


Fig. 2. Graphs of ISE potentials (mV) referenced to a Li^+ ISE and temperature ($^{\circ}\text{C}$) measured over sols 30, 32, 34, 66, 86, and 138. Sols are separated by vertical black lines, drawer open/close events are indicated by gray dashed lines, and events such as calibrant, sample, acid, and BaCl_2 addition are indicated by black dashed lines. Note: ISE potentials increase with concentration for cations, and decrease with concentration for anions.

not analyzed. The presence of HCO_3^- is suggested by the rapid increase in pH upon sample addition (Hecht et al., 2009; Kounaves et al., 2010a) and the existence of carbonate minerals in the Phoenix soil (Boynton et al., 2009; Sutter et al., 2012). Estimates of alkalinity concentrations in Phoenix soils are on the order of $1\text{--}2\text{ meq L}^{-1}$ (Marion et al., 2010; Kounaves et al., 2010a,b). Other anions that may be present in the WCL solution are chlorate (ClO_3^-) (Hanley et al., 2012) and nitrate (NO_3^-), which are commonly associated with each other and perchlorate on Earth. The perchlorate:chlorate mass ratio varies widely in terrestrial deserts, but is approximately 1:1 in caliche from the Atacama where perchlorate is closest to the high abundance on Mars (Rao et al., 2010). Furthermore, both chlorate and nitrate have recently been found in high abundance relative to perchlorate in Mars meteorite EETA79001 (Kounaves et al., 2014). We consider the possible presence of ClO_3^- , and briefly consider NO_3^- , later in our modeling results.

5. MODELING WCL SOLUTION COMPOSITIONS AND PARENT SALT ASSEMBLAGES

5.1. Possible WCL solution compositions

The relative proportions of ions measured in the WCL experiment strongly influence what salts precipitate from

solution during freezing or evaporation (Marion et al., 2010; Hanley et al., 2012) and have implications for soil minerals in equilibrium with the solution (Boynton et al., 2009; Hecht et al., 2009; Kounaves et al., 2010a,b). Due to uncertainties in the ion concentrations inferred from WCL (Table 3), we examine the spread of possible solution compositions in Rosy Red within error bounds to determine variations in the predicted parent salts. We choose Rosy Red for this analysis because it is clearly more robust than the Sorceress 1 or 2 analyses. Seven ions were measured during the Rosy Red analysis (Ca^{2+} , Mg^{2+} , Na^+ , K^+ , Cl^- , SO_4^{2-} , and ClO_4^-), excluding other ions present in the calibrant solution. If we assume that there are five possible values for each ion within error bounds (the measured value, $\pm\sigma/2$, and $\pm\sigma$), then there are 5^7 or 78,125 unique ionic combinations possible.

For each of the 78,125 possible solutions, we calculate alkalinity from charge balance and implement ion-pair corrections in PHREEQC. The ion-pair corrections were facilitated by using the RATES and KINETICS functions to adjust unpaired ion concentrations, and organizing the PHREEQC input code in Excel[®]. From these possible solutions, we exclude solutions if the alkalinity is less than zero, implying a strongly acidic soil solution. An acidic soil solution conflicts with the measured pH around 7.7. 27,512 out of the 78,125 possible solutions have an alkalinity greater

than zero. Within these 27,512 solutions, Ca^{2+} , Na^+ , K^+ , Cl^- , and ClO_4^- concentrations are uniformly distributed between the $+\sigma$, $+\sigma/2$, WCL, $-\sigma/2$, and $-\sigma$ values (Table 5). In contrast, Mg^{2+} and SO_4^{2-} concentrations have asymmetrical distributions; higher Mg^{2+} and lower SO_4^{2-} concentrations are more frequent in the possible solutions. No possible solutions have SO_4^{2-} concentrations greater than the WCL analysis (4.24 mM), which places an upper bound on SO_4^{2-} concentrations in Rosy Red. Average solute concentrations in the possible WCL solutions (including ion-pair contributions) are: $\text{Ca}^{2+} = 0.186$, $\text{Mg}^{2+} = 3.459$, $\text{Na}^+ = 1.472$, $\text{K}^+ = 0.329$, $\text{Cl}^- = 0.407$, $\text{SO}_4^{2-} = 1.511$, $\text{ClO}_4^- = 2.743$ mM, and $\text{Alk.} = 2.919$ meq.

5.2. Modeling with FREZCHEM

Parent salt compositions at the Phoenix site have been inferred from numerical equilibrium models such as FREZCHEM (Marion et al., 2010) and Geochemist's Workbench® (Hanley et al., 2012). These equilibrium models assume that salts are initially dissolved in solution and are then precipitated as the solution is concentrated by either freezing or evaporation. The presence of liquid water at the Phoenix site, both past and present, is suggested by the detection of 3–5 wt.% carbonates by the Thermal and Evolved Gas Analyzer (TEGA) (Boynton et al., 2009), the distribution of perchlorate salts throughout the soil column (Cull et al., 2010), and observations (albeit controversial) of deliquescence on the Phoenix Lander struts (Rennó et al., 2009). After the formation of a liquid solution, salts may precipitate from solution as the temperature decreases and, once temperatures drop below the eutectic, the solution will freeze. Evaporation is an alternative pathway for salt precipitation and produces different salt assemblages than freezing (Marion et al., 2010). However, there are several observations which suggest that salts at the Phoenix site precipitate during freezing: (1) concentrated solutions of ClO_4^- have low water activities and will resist evaporation (Chevrier et al., 2009), (2) soil solutions will be buffered against evaporation by overlying soil layers and ground ice, and (3) the presence of ice near the surface indicates that vapor transport in the soil is either extremely slow or is in steady state (Mellon et al., 2008, 2009; Smith et al., 2009).

Equilibrium models also assume that salts in the soil are in equilibrium with each other and with brines. Potentially, salts in Martian soils could be in disequilibrium due to the limited mobility of brines in cold-dry soils. However, the distribution of perchlorate salts in Phoenix soils suggests that salts have been redistributed throughout the soil by downward percolating brines (Cull et al., 2010). Aqueous

transport in the soil would promote equilibration by allowing salts to chemically interact with each other. Although brine transport in cold-dry soils is slow (Ugolini and Anderson, 1973; Hagedorn et al., 2010; Toner and Sletten, 2013), the assumption of equilibrium in the Phoenix soil is not unreasonable given an estimated soil age at the Phoenix site of 600 Ma (Heet et al., 2009) and inferred conditions of periodic moisture (Boynton et al., 2009).

To determine how salt phases and brine compositions will change during freezing, we use FREZCHEM to model equilibrium freezing of the average composition of possible WCL solutions (Figs. 3 and 4). This equilibrium modeling is different from fractional crystallization modeling done by Marion et al. (2010) because our model allows salts to redissolve into solution at a lower temperature after they precipitate. Between 0 and -35 °C, our modeling results are similar to modeling done by Marion et al. (2010); the solution evolves towards a primarily Na- ClO_4 -rich composition at low temperatures, with lesser components of Mg^{2+} and Cl^- . K^+ concentrations quickly decrease and stay low due to precipitation of insoluble KClO_4 . Ca^{2+} concentrations are also low due to the precipitation of $\text{CaSO}_4 \cdot 2\text{H}_2\text{O}$ and CaCO_3 , but steadily increase with decreasing temperature. Hydromagnesite is the dominant sink for alkalinity. SO_4^{2-} concentrations rapidly decrease on freezing when $\text{MgSO}_4 \cdot 11\text{H}_2\text{O}$ precipitates, which is the most prevalent soluble salt phase by weight in the Phoenix soil according to our model.

Following Marion et al. (2010), alkalinity and carbonate phases were removed below -20 °C because these phases cause convergence failures and, as noted by Marion et al. (2010), carbonate chemistries are only valid in FREZCHEM down to -22 °C. Marion et al. (2010) also removed minor Ca^{2+} , K^+ , and SO_4^{2-} from solution; however, we retain these ions. To conserve charge balance, alkalinity is assumed to precipitate as CaCO_3 , removing an equivalent amount of Ca^{2+} from solution. Below -35 °C, the solution evolves towards a Mg-Ca- ClO_4 -rich composition and is distinct from the solution compositions modeled in Marion et al. (2010). At -36.2 °C and -43.7 °C, $\text{NaClO}_4 \cdot 2\text{H}_2\text{O}$ and $\text{MgCl}_2 \cdot 12\text{H}_2\text{O}$ begin precipitating respectively, with $\text{NaClO}_4 \cdot 2\text{H}_2\text{O}$ later transitioning to $\text{NaClO}_4 \cdot \text{H}_2\text{O}$ at -45.2 °C. These salts remove Cl^- and Na^+ from solution, causing the resulting solution to become enriched in Mg^{2+} , Ca^{2+} , and ClO_4^- . Surprisingly, Ca^{2+} does not combine with SO_4^{2-} at low temperatures to precipitate $\text{CaSO}_4 \cdot 2\text{H}_2\text{O}$; instead, SO_4^{2-} is precipitated with Mg^{2+} as $\text{MgSO}_4 \cdot 11\text{H}_2\text{O}$. The formation of Ca^{2+} -rich compositions did not occur in modeling done by Marion et al. (2010) because Ca^{2+} was removed from solution at -20 °C.

Table 5

The percentage of Rosy Red solutions with a given ion concentration within $\pm 1\sigma$ of the WCL analysis in which alkalinity > 0 .

	Ca^{2+}	Mg^{2+}	Na^+	K^+	Cl^-	ClO_4^-	SO_4^{2-}
$+\sigma$	20.7	26.7	21.3	20.2	19.8	18.0	0.0
$+\sigma/2$	20.3	22.7	20.6	20.1	19.9	18.6	0.0
WCL	20.0	22.5	20.0	20.0	20.0	19.8	4.0
$-\sigma/2$	19.6	16.6	19.4	19.9	20.1	21.2	39.3
$-\sigma$	19.3	11.4	18.7	19.8	20.2	22.4	56.8

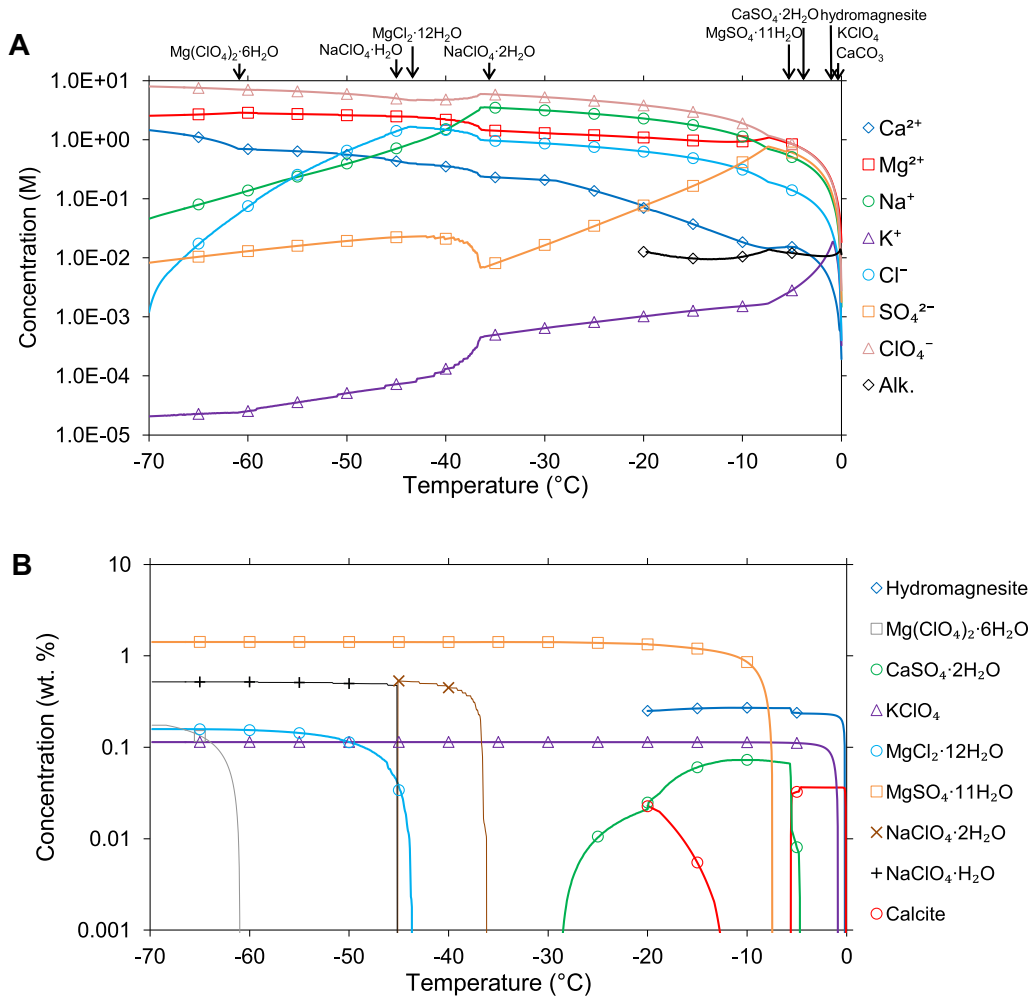


Fig. 3. (A) Ion concentrations modeled during freezing of the average composition of possible WCL solutions. (B) Salt precipitates modeled during freezing of the average composition of possible WCL solutions. Precipitates in B occur at the same temperature indicated by the arrows in A.

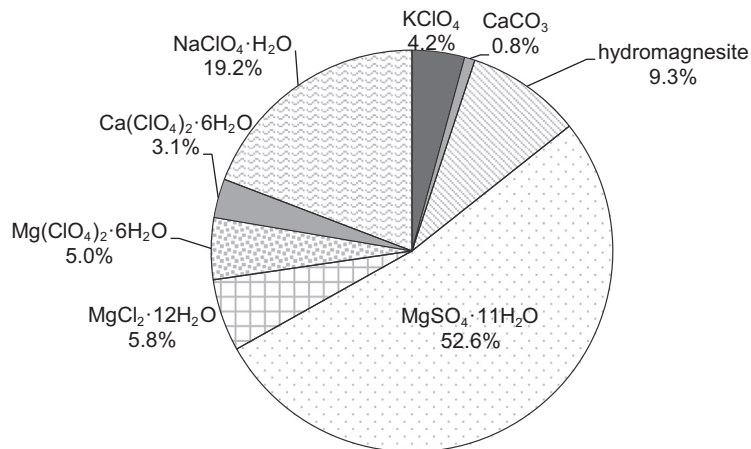


Fig. 4. The average proportion of salt phases by weight in Rosy Red inferred from FREZCHEM.

Solution compositions and salt phases are only shown to -70 °C in Fig. 3, but modeling at lower temperatures indicates that the solution continues evolving towards a more

Ca-ClO₄-rich composition and does not freeze until below -100 °C. This is much lower than the individual eutectics of either Mg(ClO₄)₂ (-68.2 °C) or Ca(ClO₄)₂ (-74.4 °C).

Although we expect that some eutectic depression will occur in mixed salt systems, a eutectic depression below $-100\text{ }^\circ\text{C}$ is probably an artifact of the model. Similarly low eutectic temperatures occur when other mixtures of aqueous $\text{Ca}(\text{ClO}_4)_2$ – $\text{Mg}(\text{ClO}_4)_2$ are modeled in FREZCHEM. These anomalously low eutectic depressions may be caused by the parameterization of the $\text{Mg}(\text{ClO}_4)_2 \cdot 6\text{H}_2\text{O}$ solubility product in FREZCHEM to the $-68\text{ }^\circ\text{C}$ eutectic determined by Dobrynina et al. (1980) and Pestova et al. (2005). Stillman and Grimm (2011) have suggested that the $-68\text{ }^\circ\text{C}$ $\text{Mg}(\text{ClO}_4)_2$ eutectic is incorrect, likely due to supercooling, and should be about $10\text{ }^\circ\text{C}$ higher at $-57\text{ }^\circ\text{C}$. Our own lab experiments confirm that solutions of $\text{Mg}(\text{ClO}_4)_2$ readily supercool and that $-57\text{ }^\circ\text{C}$ is the true eutectic (Toner et al., 2014).

There are several other reactions in Fig. 3 that run counter to experimental and modeling predictions for freezing seawater (Marion et al., 1999), surface waters (Toner and Sletten, 2013), and FREZCHEM modeling at other sites on Mars (Marion et al., 2009). Specifically, modeling done here predicts that $\text{MgCl}_2 \cdot 12\text{H}_2\text{O}$ precipitates instead of $\text{NaCl} \cdot 2\text{H}_2\text{O}$, despite the lower eutectic temperature of $\text{NaCl} \cdot 2\text{H}_2\text{O}$ ($-21.3\text{ }^\circ\text{C}$) compared to $\text{MgCl}_2 \cdot 12\text{H}_2\text{O}$ ($-33\text{ }^\circ\text{C}$), and the high concentrations of both Na^+ and Cl^- above $-35\text{ }^\circ\text{C}$. Similar reversals occur with respect to hydromagnesite vs. CaCO_3 , $\text{MgSO}_4 \cdot 11\text{H}_2\text{O}$ vs. $\text{CaSO}_4 \cdot 2\text{H}_2\text{O}$, and $\text{MgSO}_4 \cdot 11\text{H}_2\text{O}$ vs. $\text{Na}_2\text{SO}_4 \cdot 10\text{H}_2\text{O}$ precipitation; the more soluble minerals hydromagnesite and $\text{MgSO}_4 \cdot 11\text{H}_2\text{O}$ preferentially precipitate over less soluble CaCO_3 , $\text{CaSO}_4 \cdot 2\text{H}_2\text{O}$, and $\text{Na}_2\text{SO}_4 \cdot 10\text{H}_2\text{O}$. This effect is most apparent below $-50\text{ }^\circ\text{C}$, where the solution is rich in Ca^{2+} . Typically, freezing of surface waters results in Ca^{2+} -depleted solutions because HCO_3^- and SO_4^{2-} combine with Ca^{2+} to precipitate CaCO_3 and $\text{CaSO}_4 \cdot 2\text{H}_2\text{O}$ from solution (Marion et al., 2009; Toner and Sletten, 2013). However, the WCL solution evolves to a Ca^{2+} -rich composition in spite of the initially high proportions of HCO_3^- and SO_4^{2-} relative to Ca^{2+} .

The peculiar low temperature evolution of Ca– ClO_4 -rich brine modeled in FREZCHEM is caused by high Mg^{2+} activities relative to Ca^{2+} activities, which results in simultaneous ‘salting out’ and ‘salting in’ effects for salts of these ions. ‘Salting out’ occurs when the activity coefficient of an ion increases, which can cause that ion to precipitate out of solution as a salt; similarly, ‘salting in’ occurs when the activity coefficient for an ion decreases, causing that ion to either stay in solution or to dissolve into solution from a precipitated phase. For a mixed $\text{Ca}(\text{ClO}_4)_2$ – $\text{Mg}(\text{ClO}_4)_2$ brine, FREZCHEM calculates activity coefficients (γ) for Ca^{2+} and Mg^{2+} using the Pitzer equation:

$$\ln \gamma_M = z_M^2 F + m_a (2B_{Ma} + ZC_{Ma}) + \sum_c [m_c (2\Phi_{Mc} + m_a \Psi_{Mca}) + |z_M| m_c m_a C_{ca}] \quad (9)$$

where, m is a molal concentration, subscript M stands for either Ca^{2+} or Mg^{2+} , subscript c stands for a cation different from M , a stands for ClO_4^- , z_M is the cation charge, B_{Ma} and C_{Ma} are cation– ClO_4^- interaction parameters, Φ_{Mc} is the Ca^{2+} – Mg^{2+} interaction parameter, and Ψ_{Mca} is the Ca^{2+} – Mg^{2+} – ClO_4^- interaction parameter. F is a modified Debye–Hückel term and Z is an equation parameter. By

separating this equation into Debye–Hückel, cation– ClO_4^- , Ca^{2+} – Mg^{2+} , and Ca^{2+} – Mg^{2+} – ClO_4^- interaction components, we can visualize the various contributions to $\ln \gamma_M$ in $\text{Ca}(\text{ClO}_4)_2$ – $\text{Mg}(\text{ClO}_4)_2$ solutions at varying temperatures and compositions (Fig. 5).

Fig. 5 shows that cation– ClO_4^- and Ca^{2+} – Mg^{2+} interactions greatly increase at lower temperatures, causing Ca^{2+} activity coefficients to become small relative to Mg^{2+} . In a 3 molal solution dominated by Mg^{2+} at $-60\text{ }^\circ\text{C}$, $\gamma_{\text{Mg}^{2+}}/\gamma_{\text{Ca}^{2+}}$ is ~ 5000 , whereas at $25\text{ }^\circ\text{C}$, $\gamma_{\text{Mg}^{2+}}/\gamma_{\text{Ca}^{2+}}$ is ~ 2 . Such large relative differences in modeled Mg^{2+} activities relative to Ca^{2+} at low temperatures causes salts of Mg^{2+} to strongly precipitate from solution (the ‘salting out’ effect) and salts of Ca^{2+} to dissolve into solution (the ‘salting in’ effect). We note that the strong influence of Ca^{2+} – Mg^{2+} interactions on activity coefficients in FREZCHEM is surprising because Pitzer (1991) indicates that these interactions should have only a slight effect on activity coefficients. Furthermore, Silvester and Pitzer (1978) found that the temperature dependence of interaction parameters is small, but in FREZCHEM temperature dependencies can be large. For example, the change in the $B_{\text{Mg,ClO}_4}^1$ Pitzer parameter with temperature is $+0.0045\text{ }^\circ\text{C}^{-1}$ at $25\text{ }^\circ\text{C}$ based on experimental heat of dilution data (Silvester and Pitzer, 1978), which is similar to other salts. Assuming that this change can be extrapolated over a reasonable temperature range, the value of $B_{\text{Mg,ClO}_4}^1$ should decrease by 0.1 from $25\text{ }^\circ\text{C}$ to $0\text{ }^\circ\text{C}$; however, in FREZCHEM, $B_{\text{Mg,ClO}_4}^1$ increases by 2.2 over this temperature range.

Very high $\gamma_{\text{Mg}^{2+}}/\gamma_{\text{Ca}^{2+}}$ ratios in the presence of ClO_4^- suggest the possibility that at low temperatures Ca–Mg– ClO_4 -rich solutions could form because Mg^{2+} will act as a stronger sink for SO_4^{2-} and HCO_3^- than Ca^{2+} . This prediction is consistent with a recent, more in-depth analysis of the WCL Ca^{2+} ISE signal response and experimental results of ISE signals in mixed $\text{Ca}(\text{ClO}_4)_2$ – $\text{Mg}(\text{ClO}_4)_2$ solutions (Kounaves et al., 2012). Kounaves et al. (2012) found that a transient signal in the Ca^{2+} ISE suggests that about 60% of the ClO_4^- in the soil was present as $\text{Ca}(\text{ClO}_4)_2$. The salting in and salting out effects found here provide a possible theoretical framework for how a Ca– ClO_4 -rich solution might have evolved from a solution with initially high concentrations of SO_4^{2-} and HCO_3^- .

However, activity coefficients calculated by FREZCHEM are only as accurate as the experimental data used to parameterize the model. Binary Pitzer parameters for $\text{Mg}(\text{ClO}_4)_2$ and $\text{Ca}(\text{ClO}_4)_2$ used in FREZCHEM are calculated from the freezing point depression of ice in varying concentration salt solutions (Marion et al., 2010). The probable underestimation of the $\text{Mg}(\text{ClO}_4)_2$ eutectic in Dobrynina et al. (1980) and Pestova et al. (2005) suggests that the ice-solution datasets used to parameterize FREZCHEM may be inaccurate. To test how sensitive the Pitzer model is to experimental errors, we calculate Pitzer parameters and Mg^{2+} activity coefficients by assuming that the concentration of salt in equilibrium with ice varies from FREZCHEM systematically up to $\pm 10\%$ (Fig. 6). Following Marion et al. (2010), this is done by fitting the Pitzer parameters B_{Ma} and C_{Ma} to the equation $P(T) = P_{298.15} + A(298.15 - T)$

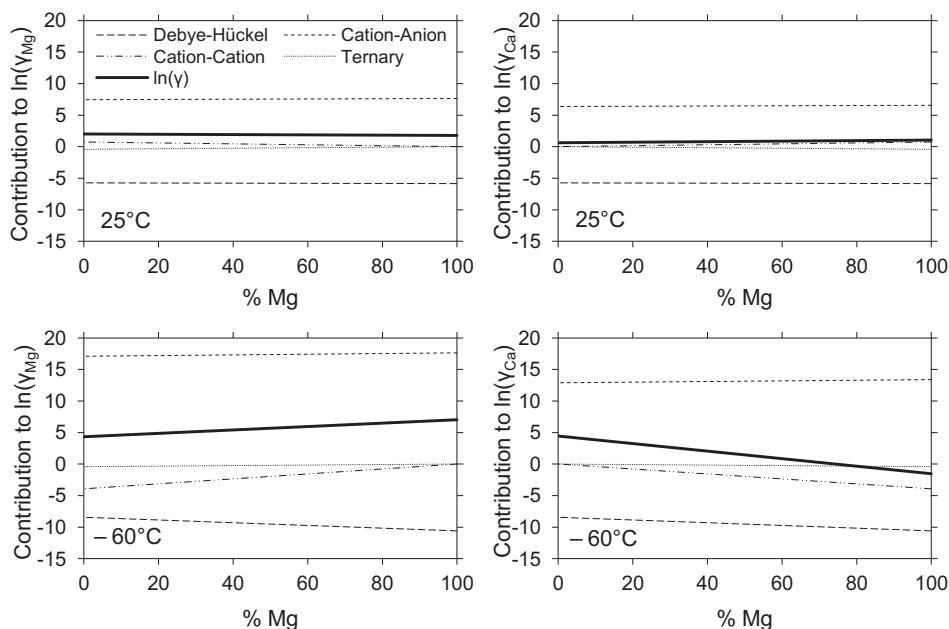


Fig. 5. Contributions to $\ln \gamma_{Ca}$ and $\ln \gamma_{Mg}$ in 3 m perchlorate solutions containing varying proportions of Ca^{2+} and Mg^{2+} at 25 °C and -60 °C, determined using Pitzer parameters from FREZCHEM. The different components of $\ln \gamma_M$ are: (1) the Debye–Hückel component, $Z_M^2 F$, (2) the cation- ClO_4^- interaction component, $m_a(2B_{Ma} + ZC_{Ma}) + \sum_c |z_M| m_c m_a C_{ca}$, (3) the Ca^{2+} - Mg^{2+} interaction component, $\sum_c 2\Phi_{Mc} m_c$, and (4) the Ca^{2+} - Mg^{2+} - ClO_4^- interaction component, $\sum_c m_c m_a \Psi_{Mca}$.

using a sum-least-squares fitting method, where $P(T)$ is the temperature-dependent Pitzer parameter, $P_{298.15}$ is the value at 298.15 K, T is the temperature in Kelvin, and A is the constant to be fitted. Mg^{2+} activity coefficients are then calculated using the new Pitzer parameters. The results of this sensitivity analysis indicate that activity coefficients are highly sensitive to errors in the experimental data, particularly at low temperatures (Fig. 6). A decrease in the experimental salt concentration values in equilibrium with ice produces an exponential increase in modeled activity coefficients. Given that freezing point depressions in Dobrynina et al. (1980) and Pestova et al. (2005) may be too low due to metastability in $Mg(ClO_4)_2$ solutions (Stillman and Grimm, 2011), the concentration of salt in equilibrium with ice at a given temperature would be higher (the blue lines in Fig. 6B, which correspond to activity coefficients in Fig. 6A). The possible experimental errors and inconsistencies mentioned above point to a need for new, highly accurate

experimental work on freezing-point depressions in pure $Mg(ClO_4)_2$ and $Ca(ClO_4)_2$ solutions, and tests of the FREZCHEM model in mixed salt systems containing ClO_4^- .

5.3. Chemical divide modeling

Ideally, all of the 27,512 possible WCL solutions could be evaluated for salt precipitates and brine compositions using FREZCHEM. However, for reasons given above, the use of perchlorate parameters in mixed salt systems needs further experimental evaluation before we can be confident of model predictions. In addition, FREZCHEM sometimes fails to converge below about -20 °C, which has been attributed to the presence of minor species at low temperatures (Marion et al., 2010). We find that convergence failures in FREZCHEM below -20 °C are caused when ClO_4^- concentrations become high in the presence of Mg^{2+} . In some cases, the activity coefficient of Mg^{2+}

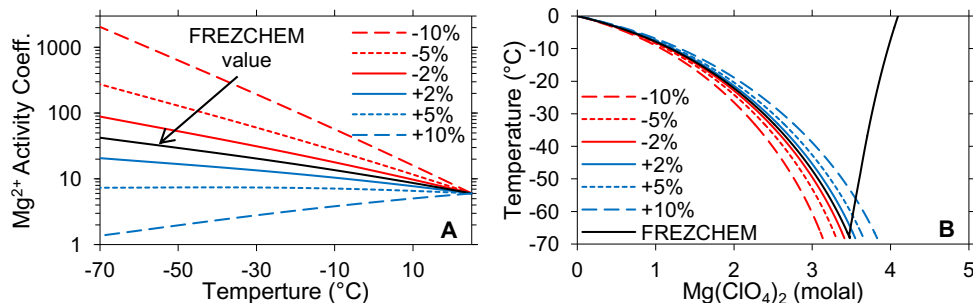


Fig. 6. (A) The variation in Mg^{2+} activity coefficients with temperature for 3 m solutions of $Mg(ClO_4)_2$ that arise if salt concentrations from experimental ice–solution data used to parameterize the Pitzer model are varied by up to $\pm 10\%$. (B) Deviations from the FREZCHEM $Mg(ClO_4)_2$ phase diagram assuming that the concentration of salt in equilibrium with ice varied up to $\pm 10\%$.

increases by a factor of around 10^5 . These convergence problems could potentially be resolved by revised $\text{Mg}(\text{ClO}_4)_2$ Pitzer parameters.

Because of the problems in numerical models, we use a chemical divide model (Hardie and Eugster, 1970; Eugster and Jones, 1979; Drever, 1982) to evaluate the parent salts of possible Rosy Red solutions. A chemical divide model has previously been applied to fluids derived from basalt weathering on Mars (Tosca and McLennan, 2006) and primordial Martian solutions (King et al., 2004). In a chemical divide model, the evolution of brines as they are concentrated is determined using a decision tree that considers the relative solubility of salts and ratios of cations to anions as the solution evolves. For example, if a solution is characterized by $\text{K}^+ < \text{ClO}_4^-$, then precipitation of insoluble KClO_4 will consume K^+ early during freezing and the solution will evolve towards a K^+ -depleted composition. The chemical divide model assumes that K^+ completely precipitates with an equivalent concentration of ClO_4^- , and the resulting solution is further evaluated for other chemical divides. If, on the other hand, $\text{K}^+ > \text{ClO}_4^-$, then the solution will become depleted in ClO_4^- after the precipitation of KClO_4 . Because the chemical divide model removes chemical species by precipitation reactions, chemical divides between species are evaluated stoichiometrically in equivalent concentrations (e.g. $2[\text{Mg}^{2+}]$ is compared to $[\text{Cl}^-]$).

5.3.1. Choosing the chemical divides

In a chemical divide model, the relative solubility of salts defines the order in which salts are removed upon concentration. Studies of evaporating closed basin lake waters on Earth have demonstrated the validity of this technique (Hardie and Eugster, 1970; Eugster and Jones, 1979). Fewer studies have been done on freezing waters, but in freezing seawater, salts with higher eutectic temperatures precipitate before salts with lower eutectic temperatures (Gitterman, 1937; Nelson and Thompson, 1954; Herut et al., 1990). This suggests that a chemical divide model for freezing waters can be based on relative eutectic temperatures; however, a potential complication to this is that salts may redissolve into solution at temperatures lower than their eutectics due to changes in ion activities or solubility products with temperature. FREZCHEM suggests that $\text{Na}_2\text{SO}_4 \cdot 10\text{H}_2\text{O}$, CaCO_3 , and $\text{CaSO}_4 \cdot 2\text{H}_2\text{O}$ will redissolve into solution

when WCL solutions are frozen to low temperatures, but these effects are likely influenced by an overestimation of Mg^{2+} activities, as discussed previously. Furthermore, with the exception of $\text{Na}_2\text{SO}_4 \cdot 10\text{H}_2\text{O}$, experimental freezing of seawater indicates that salts do not redissolve into solution at lower temperatures once they have precipitated (Marion et al., 1999).

In a system containing the ions Cl^- , SO_4^{2-} , HCO_3^- , and ClO_4^- , the eutectic temperature of salts in order of decreasing temperature is generally given by: carbonates > sulfates > chlorides > perchlorates (Table 6). KClO_4 (-0.18°C), NaHCO_3 , (-2.76°C), and KHCO_3 (-6.38°C) are notable exceptions to this rule, although highly soluble Na–K-carbonates are unlikely to form because HCO_3^- preferentially precipitates with Ca^{2+} or Mg^{2+} first. K^+ will be consumed early during freezing because it is a minor soil constituent and is strongly precipitated as insoluble KClO_4 from a Phoenix WCL solution (Marion et al., 2010). Soluble Ca^{2+} is also minor in the Phoenix WCL solution and will be consumed by precipitation in CaCO_3 first, followed by precipitation of any remaining Ca^{2+} in $\text{CaSO}_4 \cdot 2\text{H}_2\text{O}$. Although CaCO_3 and CaSO_4 can precipitate in various hydrated states, such as ikaite ($\text{CaCO}_3 \cdot 6\text{H}_2\text{O}$), anhydrite (CaSO_4), or basanite ($\text{CaSO}_4 \cdot 1.5\text{H}_2\text{O}$), this does not affect the continuing evolution of brines in a chemical divide model because the ratio of cations to anions in different hydrated salts is the same. Mg^{2+} will then combine with any remaining alkalinity after CaCO_3 precipitation, which quantitatively removes alkalinity from solution. Assuming that anhydrous magnesite (MgCO_3) does not form on Mars during freezing due to kinetic inhibition at low temperatures (Langmuir, 1965; Marion et al., 2010), FREZCHEM predicts that Mg^{2+} will precipitate with HCO_3^- as hydromagnesite. However, because hydrous MgCO_3 minerals are poorly characterized at low temperatures, and the hydrated state depends on the pCO_2 and pH, we denote the hydrous MgCO_3 mineral in our chemical divide model as $\text{MgCO}_3 \cdot n\text{H}_2\text{O}$.

After the precipitation of minor Ca^{2+} , K^+ , and alkalinity in KClO_4 , CaCO_3 , $\text{CaSO}_4 \cdot 2\text{H}_2\text{O}$, and $\text{MgCO}_3 \cdot n\text{H}_2\text{O}$, the remaining solution will have a Mg–Na–Cl– ClO_4 – SO_4 composition. This simplifies the chemical divide model considerably. Based on the relative eutectic temperatures of salts, the order of salt precipitation from a Mg–Na–Cl–

Table 6
Eutectic temperatures ($^\circ\text{C}$) and solid phase eutectic salts for binary salt systems modeled in FREZCHEM, except where otherwise noted.

	Ca^{2+}		Mg^{2+}		Na^+		K^+	
CO_3^{2-}	CaCO_3	–0.006	Hydromagnesite	–0.2	NaHCO_3	–2.8	KHCO_3	–6.4
SO_4^{2-}	$\text{CaSO}_4 \cdot 2\text{H}_2\text{O}$	–0.03	$\text{MgSO}_4 \cdot 11\text{H}_2\text{O}$	–3.6	$\text{Na}_2\text{SO}_4 \cdot 10\text{H}_2\text{O}$	–1.2	K_2SO_4	–1.5
Cl^-	$\text{CaCl}_2 \cdot 6\text{H}_2\text{O}$	–49.4	$\text{MgCl}_2 \cdot 12\text{H}_2\text{O}$	–33.0	$\text{NaCl} \cdot 2\text{H}_2\text{O}$	–21.3	KCl	–10.8
ClO_3^-	$\text{Ca}(\text{ClO}_3)_2 \cdot 6\text{H}_2\text{O}$	–41 ^b	$\text{Mg}(\text{ClO}_3)_2 \cdot 6\text{H}_2\text{O}$	–69 ^b	NaClO_3	–23 ^b	KClO_3	–3 ^b
ClO_4^-	$\text{Ca}(\text{ClO}_4)_2 \cdot 6\text{H}_2\text{O}$	–74.4	$\text{Mg}(\text{ClO}_4)_2 \cdot 6\text{H}_2\text{O}^c$	–57 ^a	$\text{NaClO}_4 \cdot 2\text{H}_2\text{O}$	–34.3	KClO_4	–0.18
NO_3^-	$\text{Ca}(\text{NO}_3)_2 \cdot 4\text{H}_2\text{O}$	–28.7 ^c	$\text{Mg}(\text{NO}_3)_2 \cdot 9\text{H}_2\text{O}$	–31.9 ^d	NaNO_3	–17.6	KNO_3	–2.9

^a Stillman and Grimm (2011).

^b Hanley et al. (2012).

^c Bassett and Taylor (1912).

^d Ewjing et al. (1933).

^e Marion et al. (2010) is uncertain whether this salt has 6 or 8 waters of hydration. We assume a hydrated state of $6\text{H}_2\text{O}$ because this is consistent with the hydrated state at 25°C .

$\text{ClO}_4\text{-SO}_4$ solution will be given by $\text{Na}_2\text{SO}_4\cdot 10\text{H}_2\text{O}$, $\text{MgSO}_4\cdot 11\text{H}_2\text{O}$, $\text{NaCl}\cdot 2\text{H}_2\text{O}$, $\text{MgCl}_2\cdot 12\text{H}_2\text{O}$, $\text{NaClO}_4\cdot 2\text{H}_2\text{O}$, and $\text{Mg}(\text{ClO}_4)_2\cdot 6\text{H}_2\text{O}$, in order from first to last. Although this precipitation sequence indicates that $\text{Na}_2\text{SO}_4\cdot 10\text{H}_2\text{O}$ precipitates before $\text{MgSO}_4\cdot 11\text{H}_2\text{O}$, once temperatures decrease to the point where $\text{NaCl}\cdot 2\text{H}_2\text{O}$ or $\text{NaClO}_4\cdot 2\text{H}_2\text{O}$ begin precipitating, Na^+ concentrations will decrease. This will cause any $\text{Na}_2\text{SO}_4\cdot 10\text{H}_2\text{O}$ that had precipitated to redissolve into solution. The SO_4^{2-} released by $\text{Na}_2\text{SO}_4\cdot 10\text{H}_2\text{O}$ will then combine with Mg^{2+} to precipitate $\text{MgSO}_4\cdot 11\text{H}_2\text{O}$. Because Mg^{2+} concentrations are high in the WCL solutions, this reaction will continue until either all of the Mg^{2+} has been precipitated as $\text{MgSO}_4\cdot 11\text{H}_2\text{O}$ or all of the $\text{Na}_2\text{SO}_4\cdot 10\text{H}_2\text{O}$ has dissolved. A similar effect, in which $\text{Na}_2\text{SO}_4\cdot 10\text{H}_2\text{O}$ redissolves into solution after $\text{NaCl}\cdot 2\text{H}_2\text{O}$ begins precipitating, occurs in seawater (Marion et al., 1999). As a result, $\text{Na}_2\text{SO}_4\cdot 10\text{H}_2\text{O}$ and $\text{MgSO}_4\cdot 11\text{H}_2\text{O}$ can be thought of as effectively precipitating after $\text{NaCl}\cdot 2\text{H}_2\text{O}$ and $\text{NaClO}_4\cdot 2\text{H}_2\text{O}$ in a chemical divide model. Possibly, mixed $\text{Na}_2\text{SO}_4\text{-MgSO}_4$ salts could precipitate from solution, such as bloedite ($\text{Na}_2\text{SO}_4\cdot \text{MgSO}_4\cdot 4\text{H}_2\text{O}$); however, we do not consider such salts in our low temperature modeling because bloedite is unstable at low temperatures (Marion and Farren, 1999).

5.3.2. Chemical divide model results

When the chemical divide model outlined above is applied to all of the 27,512 possible Rosy Red WCL solutions, only two, similar evolution pathways are followed (Fig. 7). Ca^{2+} is removed early as both CaCO_3 and sometimes $\text{CaSO}_4\cdot 2\text{H}_2\text{O}$, followed by K^+ as KClO_4 . Here, the chemical divide model indicates that the possible solutions diverge slightly. If $2\text{Ca}^{2+} > \text{Alk.}$, then alkalinity is completely consumed by CaCO_3 precipitation and excess Ca^{2+} precipitates as $\text{CaSO}_4\cdot 2\text{H}_2\text{O}$; on the other hand, if $2\text{Ca}^{2+} < \text{Alk.}$, then Ca^{2+} is completely consumed by CaCO_3 precipitation and excess alkalinity precipitates as $\text{MgCO}_3\cdot n\text{H}_2\text{O}$. Following the precipitation of Ca^{2+} and alkalinity, all of the possible WCL solutions in the chemical divide model have a similar Mg-Na-Cl-ClO_4 composition and follow the same evolution pathway.

The most common WCL evolution pathway (92.3% of the possible solutions) results in a final parent salt composition of $\text{MgSO}_4\cdot 11\text{H}_2\text{O}$, $\text{MgCO}_3\cdot n\text{H}_2\text{O}$, $\text{Mg}(\text{ClO}_4)_2\cdot 6\text{H}_2\text{O}$, $\text{NaClO}_4\cdot 2\text{H}_2\text{O}$, KClO_4 , $\text{NaCl}\cdot 2\text{H}_2\text{O}$, and CaCO_3 , in order of mass abundance (Table 7 and Fig. 8A). All of the possible WCL solutions precipitate KClO_4 , CaCO_3 , $\text{MgSO}_4\cdot 11\text{H}_2\text{O}$, $\text{NaCl}\cdot 2\text{H}_2\text{O}$, $\text{NaClO}_4\cdot 2\text{H}_2\text{O}$, and $\text{Mg}(\text{ClO}_4)_2\cdot 6\text{H}_2\text{O}$. $\text{MgSO}_4\cdot 11\text{H}_2\text{O}$ is the most prevalent salt phase present in the Phoenix soil and comprises 1.2 wt.% of the soil on average. The weight fraction for CaCO_3 is much lower than estimates of 3–5 wt.% CaCO_3 based on a high temperature CO_2 release measured in TEGA (Boynton et al., 2009). This is not surprising because CaCO_3 is sparingly soluble and would have only partially dissolved into solution. In contrast, highly soluble salts such as $\text{Mg}(\text{ClO}_4)_2\cdot 6\text{H}_2\text{O}$ and $\text{NaClO}_4\cdot 2\text{H}_2\text{O}$ would have completely dissolved and represent the actual concentration of these salts in the soil.

On a mole fraction basis, $\text{MgSO}_4\cdot 11\text{H}_2\text{O}$ is the dominant sink for SO_4^{2-} in the possible WCL solutions,

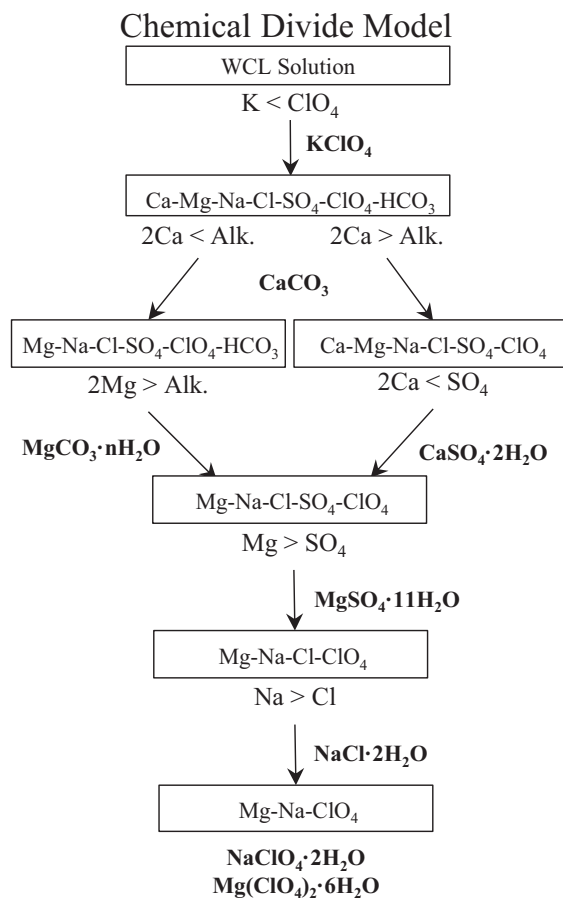


Fig. 7. The evolution pathways for possible Rosy Red WCL solutions in a chemical divide model based largely on the relative eutectic temperature of component salts. Only pathways taken by the possible WCL solutions are shown.

averaging 99.4 mol% of the SO_4^{2-} . $\text{MgCO}_3\cdot n\text{H}_2\text{O}$ is the dominant sink for alkalinity, averaging 87.8 mol% of the alkalinity, followed by CaCO_3 (averaging 12.2 mol%). The inferred dominance of the $\text{MgCO}_3\cdot n\text{H}_2\text{O}$ form of carbonate is consistent with orbital IR observations of Martian dust from the Mars Global Surveyor Thermal Emission Spectrometer (Bandfield et al., 2003) as well as outcrops of magnesium-rich carbonate observed with the Compact Reconnaissance Imaging Spectrometer for Mars (CRISM) (Ehlmann et al., 2008) and instruments on the Spirit Rover (Morris et al., 2010). Of the perchlorate salts, KClO_4 averages 12.0 mol%, $\text{NaClO}_4\cdot 2\text{H}_2\text{O}$ averages 38.8 mol%, and $\text{Mg}(\text{ClO}_4)_2\cdot 6\text{H}_2\text{O}$ averages 49.2 mol% of the ClO_4^- . Cl^- is completely precipitated as $\text{NaCl}\cdot 2\text{H}_2\text{O}$, a mineral that is present in all of the possible WCL solutions and has not been previously considered at the Phoenix site.

How might the existence of the chlorate (ClO_3^-) ion in the Phoenix soil affect the parent salt chemistry? Based on analyses of $\text{ClO}_3^-/\text{ClO}_4^-$ ratios on Earth by Rao et al. (2010), we consider molar equivalent amounts of ClO_3^- and ClO_4^- on Mars. We incorporate this possibility into our Rosy Red chemical divide model by adding in ClO_3^- to the possible solutions so that $\text{ClO}_3^- = \text{ClO}_4^-$, and adjust the solution for charge balance by removing alkalinity.

Table 7

Results from the chemical divide modeling both without ClO_3^- in the WCL solutions and assuming equal concentrations of ClO_3^- and ClO_4^- . Values given are the % occurrence of salt phases in possible Rosy Red solutions and the average weight% ($100 \times g_{\text{salt}} \cdot g_{\text{soil}}^{-1}$) assuming a soil mass of 1 g and a soil density of 1 g cm^{-3} . The standard deviation of the weight% in the possible solutions is also given. To calculate the weight fraction of $\text{MgCO}_3 \cdot n\text{H}_2\text{O}$, the molecular weight of hydromagnesite is assumed (365.3 g).

Salt phase	Without ClO_3^-		$\text{ClO}_3^- = \text{ClO}_4^-$	
	% occurrence	Weight %	% occurrence	Weight %
KClO_4	100	0.114 ± 0.011	100	0.114 ± 0.011
CaCO_3	100	0.044 ± 0.015	100	0.046 ± 0.015
$\text{CaSO}_4 \cdot 2\text{H}_2\text{O}$	7.7	0.004 ± 0.015	15.6	0.007 ± 0.020
$\text{MgCO}_3 \cdot n\text{H}_2\text{O}$	92.3	1.171 ± 0.788	84.4	0.602 ± 0.522
$\text{NaCl} \cdot 2\text{H}_2\text{O}$	100	0.096 ± 0.007	100	0.096 ± 0.007
NaClO_3	–	–	100	0.288 ± 0.063
$\text{NaClO}_4 \cdot 2\text{H}_2\text{O}$	100	0.422 ± 0.094	–	–
$\text{MgSO}_4 \cdot 11\text{H}_2\text{O}$	100	1.197 ± 0.785	100	0.752 ± 0.495
$\text{Mg}(\text{ClO}_3)_2 \cdot 6\text{H}_2\text{O}$	–	–	100	0.591 ± 0.153
$\text{Mg}(\text{ClO}_4)_2 \cdot 6\text{H}_2\text{O}$	100	0.559 ± 0.177	100	0.966 ± 0.141

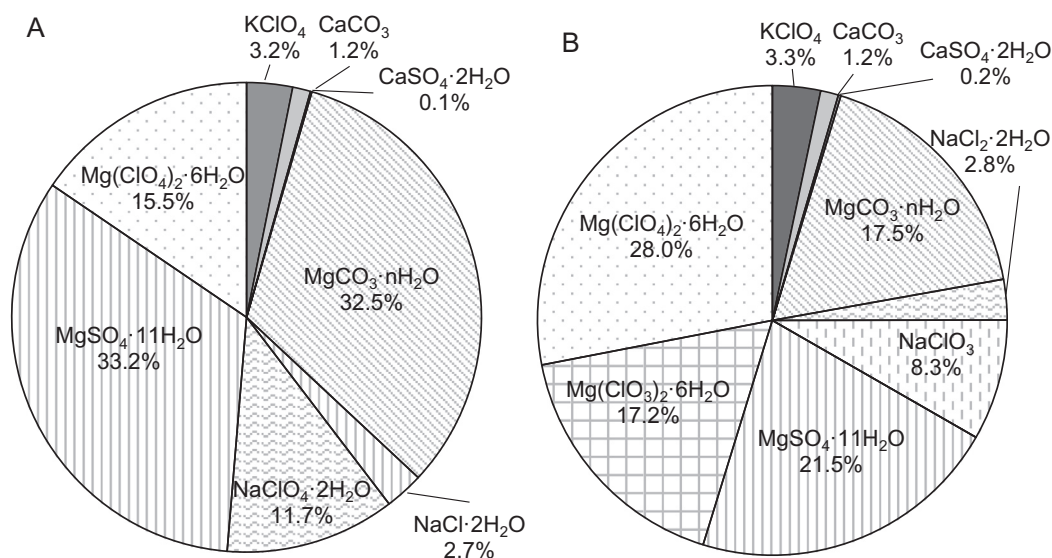


Fig. 8. (A) The average proportion of salt phases by weight in Rosy Red inferred from the chemical divide model without ClO_3^- , and (B) assuming that the ClO_3^- concentration is the same as the ClO_4^- concentration in the initial solution.

With the addition of ClO_3^- ion, a total of 13,901 possible WCL solutions have an alkalinity greater than zero. Applying the chemical divide model based on relative eutectic temperatures, the modeled parent salt assemblages are similar to assemblages modeled in the absence of ClO_3^- (Table 7 and Fig. 8B), with several exceptions. All of the Na^+ precipitates as NaClO_3 instead of $\text{NaClO}_4 \cdot 2\text{H}_2\text{O}$ due to the higher eutectic temperature of NaClO_3 (-23°C) compared to $\text{NaClO}_4 \cdot 2\text{H}_2\text{O}$ (-34.3°C). This frees all of the ClO_4^- to precipitate with Mg^{2+} as $\text{Mg}(\text{ClO}_4)_2 \cdot 6\text{H}_2\text{O}$. Furthermore, some of the residual ClO_3^- after the precipitation of NaClO_3 precipitates as $\text{Mg}(\text{ClO}_3)_2 \cdot 6\text{H}_2\text{O}$. The lower alkalinity caused by the addition of ClO_3^- in the possible WCL solutions also lowers the amount of Mg^{2+} that precipitates as $\text{MgCO}_3 \cdot n\text{H}_2\text{O}$, which frees more Mg^{2+} to precipitate as $\text{Mg}(\text{ClO}_4)_2 \cdot 6\text{H}_2\text{O}$ and $\text{Mg}(\text{ClO}_3)_2 \cdot 6\text{H}_2\text{O}$.

We do not explicitly model the possible presence of NO_3^- here because its concentration at the Phoenix site is not known. Qualitatively, the inclusion of nitrates in a chemical

divide model would have the greatest impact on chloride salts because the eutectic temperatures of Mg^{2+} and Na^+ chlorides are similar, but slightly lower than, Mg^{2+} and Na^+ nitrates. As a result, Na^+ in the WCL solutions would precipitate as NaNO_3 instead of $\text{NaCl} \cdot 2\text{H}_2\text{O}$, and any remaining Cl^- after the precipitation of $\text{NaCl} \cdot 2\text{H}_2\text{O}$ would precipitate as $\text{MgCl}_2 \cdot 12\text{H}_2\text{O}$.

The results of our chemical divide modeling indicate the equilibrium salt composition if the soil solution is frozen below its eutectic, i.e. there is no brine component in Table 7. Above the eutectic, a eutectic solid will melt to form a mixture of salt, ice, and brine. Although a chemical divide model cannot predict precise brine compositions above the eutectic, the general composition of brines can be inferred by considering the solubility and eutectic temperatures of the various salt components in the eutectic mixture. The salts having the lowest eutectic temperatures in our chemical divide modeling are $\text{Mg}(\text{ClO}_4)_2 \cdot 6\text{H}_2\text{O}$ (-57°C) and $\text{Mg}(\text{ClO}_3)_2 \cdot 6\text{H}_2\text{O}$ (-69°C), indicating that liquid brine

can form at the Phoenix site near $-57\text{ }^{\circ}\text{C}$ or $-69\text{ }^{\circ}\text{C}$. After this, $\text{NaClO}_4\cdot 2\text{H}_2\text{O}$ ($-34.3\text{ }^{\circ}\text{C}$) and NaClO_3 ($-23\text{ }^{\circ}\text{C}$) have the next lowest eutectic temperatures. This implies that between $-57\text{ }^{\circ}\text{C}$ and $-34.3\text{ }^{\circ}\text{C}$, or $-69\text{ }^{\circ}\text{C}$ and $-23\text{ }^{\circ}\text{C}$ if chlorate is included in the model, the brine composition will be Mg– ClO_4 – ClO_3 -rich. Above these temperatures, Na^+ salts will begin to dissolve, and the brine composition will become Mg–Na– ClO_4 – ClO_3 -rich. The formation of Ca–Mg-rich chloride, nitrate, chlorate, and/or perchlorate brines on Mars is significant because such brines have much lower eutectic temperatures than comparable solutions of Na^+ or K^+ . As a general rule, chemical divide models predict that low-temperature Ca–Mg-rich brines will form only when Ca^{2+} and Mg^{2+} in the soil solution exceeds equivalent concentrations of alkalinity and SO_4^{2-} i.e. $2[\text{Ca}^{2+}] + 2[\text{Mg}^{2+}] > 2[\text{SO}_4^{2-}] + [\text{Alk.}]$ (Toner and Sletten, 2013).

5.4. Implications for Mars

Hydrated salts can hold a significant quantity of water in their crystal structure, which has been discussed by many authors in the context of water reservoirs and the water cycle on Mars (Vaniman et al., 2004; Feldman et al., 2004a; Steiger et al., 2011; Stillman and Grimm, 2011). Based on the hydrated salts predicted by the chemical divide model, the soluble salts are composed of about 40% water by weight. This translates to 1.3 wt.% of the water in the Phoenix soil, assuming that $\sim 1\text{ g}$ of soil was added to the Rosy Red WCL experiment. Additional water could also be present in brines. The minimum bound water content of 1.3 wt.% inferred in the Phoenix soils is consistent with estimates of water between 1.5 and 7.5 wt.% in non-icy regions of Mars ($\pm\sim 45^\circ$ latitudes) determined by gamma-ray spectroscopy (Boynton et al., 2007), estimates of 2–9.8 wt.% water from the Neutron Spectrometer aboard Mars Odyssey (Feldman et al., 2004b), and recent measurements of soil water contents of 1.5–3 wt.% by the Sample Analysis on Mars (SAM) instrument on the Mars Science Laboratory (MSL) (Leshin et al., 2013; Ming et al., 2013). Most of the water in the WCL-inferred salts is held in the highly hydrated mineral $\text{MgSO}_4\cdot 11\text{H}_2\text{O}$. Although modeling in FREZCHEM predicts that $\text{MgSO}_4\cdot 11\text{H}_2\text{O}$ will precipitate from solution, this mineral could dehydrate under lower relative humidity and higher temperature conditions to epsomite, starkeyite, or kieserite (Steiger et al., 2011). This would lower our estimate of the bound crystalline water content in the soil. Water bound in crystalline salts could be adsorbed or released on diurnal, yearly, and orbital timescales.

In addition to binding water in their crystal structure, salts can deliquesce and draw water from the atmosphere to form liquid brine. Deliquescent salts are thought to have been observed as globules on the Phoenix Lander struts that changed position over the course of the mission (Rennó et al., 2009), and the distribution of perchlorates in the soil column suggests that salts have migrated as brines (Cull et al., 2010). Furthermore, the water measured by MSL is thought to be held in an amorphous soil component based on its release at low temperatures (Leshin et al., 2013; Ming et al., 2013) and X-ray diffraction (XRD)

results (Bish et al., 2013). Given that the amorphous component is thought to contain all of the soil Cl (Blake et al., 2013), we speculate that this water-rich, amorphous component is at least partly composed of deliquescent perchlorate brine. The soil Cl concentration measured by MSL comprises 0.61 wt.% of the soil, which is comparable to 0.28 wt.% soluble Cl^- measured by WCL in the Phoenix soil from both Cl^- and ClO_4^- .

The relative humidity at which salts will deliquesce is dependent on the salt phase, and of our modeled salt phases $\text{NaClO}_4\cdot 2\text{H}_2\text{O}$, $\text{Mg}(\text{ClO}_4)_2\cdot 6\text{H}_2\text{O}$, and $\text{Mg}(\text{ClO}_3)_2\cdot 6\text{H}_2\text{O}$ are the most deliquescent salts. Equilibrium models predict that once these salts deliquesce to a brine, they could remain liquid to temperatures as low as $-69\text{ }^{\circ}\text{C}$, in the case of $\text{Mg}(\text{ClO}_3)_2\cdot 6\text{H}_2\text{O}$, due to freezing point depression (Chevrier et al., 2009; Marion et al., 2010; Hanley et al., 2012). Stability regions inferred from equilibrium models represent the minimum temperature and relative humidity conditions under which brines can remain liquid. This is because brines can persist in metastable states when temperatures drop below their eutectic (Stillman and Grimm, 2011; Toner et al., in review), and will resist salt precipitation during evaporation due to metastable depression of their efflorescence relative humidity by up to 20–40% (Gough et al., 2011). Evaporation of water and precipitation of salts from brines will be further retarded by the slow kinetics of water evaporation from concentrated solutions (Sears and Chittenden, 2005; Altheide et al., 2009; Chevrier et al., 2009). Over diurnal cycles, these effects could preserve brines from completely dehydrating until higher relative humidity conditions during the nighttime rehydrated the brines.

The persistence of perchlorate brines on the surface of Mars has several implications for Martian surface chemistry. With respect to the habitability of Martian soils for putative life, past or present, salt rich brines could act as a stable liquid medium supporting growth and perchlorate could be used as an energy source (Coates and Achenbach, 2004). Perchlorates potentially confound attempts to find organic molecules on Mars through the oxidation of organics in pyrolysis experiments (Navarro-González et al., 2010). Secondary mineral formation in the Martian regolith may be facilitated by perchlorate-rich brines, which are likely reactive despite low Martian temperatures due to the high activities of ions in concentrated solutions. Concentrated, low temperature brines are thought to result in extensive mineral alterations in the nearest Earth-analog to Mars, the Antarctic Dry Valleys (Ugolini and Anderson, 1973; Dickinson and Rosen, 2003). The formation of brine when ice comes into contact with perchlorate could also be important for the flow of ice in the polar caps (Fisher et al., 2010; Lenferink et al., 2013).

6. CONCLUSIONS

The composition of soluble salts in Martian soils has implications for the stability of liquid water, CO_2 and H_2O sequestration in the regolith, past geochemical environments, and habitability. We determined probable salt compositions at the Phoenix site by reanalyzing WCL data

using improvements to original analyses, such as Kalman optimal smoothing, reanalysis of Earth-based calibration data, and ion-pair corrections. In the interests of unselfish cooperation in research, an example of a processing program in the freeware statistical package 'R' for analyzing the WCL data is freely available from the authors. Significantly, the incorporation of ion-pair corrections increases Mg^{2+} and Ca^{2+} concentrations in the WCL solutions (primarily due to SO_4^{2-} ion pairs) and correcting for calibration salts already present in solution lowers Ca^{2+} and Cl^- concentrations. In general, our results for Rosy Red are consistent with previous analyses of an alkaline Mg–Na– SO_4 – ClO_4 -rich solution, but ion concentrations for Sorceresses 1 and 2 are significantly different. These differences are likely due to the greater noise in the Sorceresses 1 and 2 experiments and the Kalman smoothing method we employ. Compared to Sorceresses 1 and 2, Rosy Red has much lower noise levels, is minimally affected by fluctuations in the ORP, and behaves in a manner consistent with a nominal WCL experiment. Hence, Rosy Red represents the best analysis of the Phoenix soil soluble chemistry.

To determine what salts were initially in Phoenix soils before their dissolution in the WCL solution, we applied the equilibrium freezing model FREZCHEM to possible Rosy Red WCL compositions within error bounds of our reduced WCL data. FREZCHEM predicts that brines enriched in $Ca(ClO_4)_2$ will evolve at low temperatures due to very high $\gamma_{Mg^{2+}}/\gamma_{Ca^{2+}}$ ratios, which cause salts of Mg^{2+} to be strongly 'salted out' over salts of Ca^{2+} and Na^+ . However, these anomalous results are likely caused by errors in experimental data used to parameterize FREZCHEM. As an alternative method to determine parent salt compositions, we use a chemical divide model based on the relative eutectic temperature of salts. Our chemical divide model indicates that the most probable parent salts at the Phoenix site in order of mass abundance are $MgSO_4 \cdot 11H_2O$, $MgCO_3 \cdot nH_2O$, $Mg(ClO_4)_2 \cdot 6H_2O$, $NaClO_4 \cdot 2H_2O$, $KClO_4$, $NaCl \cdot 2H_2O$, and $CaCO_3$. In all of the WCL solutions we model, $Mg(ClO_4)_2 \cdot 6H_2O$ precipitates from solution, and if the possible occurrence ClO_3^- is modeled, a mixture of $Mg(ClO_4)_2 \cdot 6H_2O$ and $Mg(ClO_3)_2 \cdot 6H_2O$ forms. $Mg(ClO_4)_2 \cdot 6H_2O$ and $Mg(ClO_3)_2 \cdot 6H_2O$ salts have eutectic

Table A.1

The reference Li ISE used (Ref), the calibration and analysis time windows used to calculate concentrations (LMST), the calibration temperature (T), the calibration ISE potential (E_c), the calibration ISE slope corrected for temperature T (S_m), and the calibration intercept (E_I) given by $E_I = E_C - S_M \log a_C$.

	Ref	Calibration interval (LMST)	Analysis Interval (LMST)	Calibration			
				T (°C)	E_c (mV)	S_m (mV dec ⁻¹)	E_I (mV)
<i>Rosy Red (sol 30)</i>							
pH _a	Li _B	10:30:47–10:34:49	12:37:29–12:46:26	−0.3 ± 0.5	134.0 ± 0.4	51.7 ± 0.4	395.8 ± 2.2
pH _b	Li _B	–	–	–	–	–	–
pH _{irid}	Li _B	11:46:46–11:55:44	13:15:07–13:44:29	5.6 ± 0.3	375.7 ± 0.8	49.5 ± 0.4	638.5 ± 2.1
Ca ²⁺	Li _B	11:46:46–11:55:44	12:37:29–12:46:26	5.6 ± 0.3	64.6 ± 0.2	27.5 ± 0.8	187.0 ± 3.5
Mg ²⁺	Li _B	11:46:46–11:55:44	12:37:29–12:46:26	5.6 ± 0.3	11.2 ± 0.3	27.1 ± 0.6	133.9 ± 2.8
Na ⁺	Li _B	11:46:46–11:55:44	12:37:29–12:46:26	5.6 ± 0.3	−69.3 ± 0.2	50.6 ± 0.9	157.6 ± 4.1
K ⁺	Li _B	11:46:46–11:55:44	12:37:29–12:46:26	5.6 ± 0.3	−92.9 ± 0.8	55.7 ± 0.6	157.1 ± 2.7
NH ₄ ⁺	Li _B	11:46:46–11:55:44	12:37:29–12:46:26	5.6 ± 0.3	−66.6 ± 0.2	56.3 ± 0.7	186.1 ± 3.2
Cl [−]	Li _B	11:46:46–11:55:44	12:37:29–12:46:26	5.6 ± 0.3	335.1 ± 0.5	−51.9 ± 0.3	141.1 ± 1.2
ClO ₄ [−]	Li _A	11:46:46–11:55:44	12:37:29–12:46:26	5.6 ± 0.3	273.6 ± 0.7	−58.6 ± 0.7	−77.7 ± 4.0
<i>Sorceress 1 (sol 41)</i>							
pH _a	Li _A	10:41:20–10:43:06	12:43:37–12:54:18	0.7 ± 0.6	125.2 ± 0.6	55.1 ± 0.4	403.9 ± 2.1
pH _b	Li _A	10:38:26–10:43:06	12:43:37–12:54:18	−0.1 ± 1.0	124.2 ± 0.3	55.3 ± 0.4	404 ± 2.3
pH _{irid}	Li _A	12:04:01–12:11:24	12:43:37–12:54:18	5.7 ± 1.1	416.6 ± 4.1	53.3 ± 0.4	619.7 ± 4.4
Ca ²⁺	Li _A	12:04:01–12:11:24	12:43:37–12:54:18	5.7 ± 1.1	159.1 ± 1.7	27.3 ± 0.6	280.3 ± 3
Mg ²⁺	Li _B	12:04:01–12:11:24	12:43:37–12:54:18	5.7 ± 1.1	−9.4 ± 0.6	26.6 ± 0.7	111 ± 3.3
Na ⁺	Li _A	12:04:01–12:11:24	12:43:37–12:54:18	5.7 ± 1.1	−57.1 ± 0.7	50.0 ± 0.5	167 ± 2.2
K ⁺	Li _A	12:04:01–12:11:24	12:43:37–12:54:18	5.7 ± 1.1	−57.9 ± 1.3	55.8 ± 1.4	192.4 ± 6.6
NH ₄ ⁺	Li _A	12:04:01–12:11:24	12:43:37–12:54:18	5.7 ± 1.1	−42.1 ± 1.1	55.9 ± 1.0	209 ± 4.7
Cl [−]	Li _B	12:04:01–12:11:24	12:43:37–12:54:18	5.7 ± 1.1	348.7 ± 1.5	−51.3 ± 0.3	156.8 ± 1.9
ClO ₄ [−]	Li _B	12:04:01–12:11:24	12:43:37–12:54:18	5.7 ± 1.1	263.5 ± 1.5	−58.6 ± 0.7	−87.9 ± 4.5
<i>Sorceress 2 (sol 107)</i>							
pH _a	Li _A	13:44:53–15:01:13	16:02:01–16:30:34	10.2 ± 0.2	−29.5 ± 1.1	55.8 ± 0.3	266.8 ± 2.0
pH _b	Li _A	13:44:53–15:01:13	16:02:01–16:30:34	10.2 ± 0.2	18.7 ± 3.6	53.6 ± 0.3	303.2 ± 4.0
pH _{irid}	Li _A	13:44:53–15:01:13	16:02:01–16:30:34	10.2 ± 0.2	210.2 ± 3.8	50.3 ± 0.4	477.4 ± 4.4
Ca ²⁺	Li _A	13:44:53–15:01:13	16:02:01–16:30:34	10.2 ± 0.2	134.1 ± 3.7	27.9 ± 0.3	258.2 ± 3.9
Mg ²⁺	Li _B	13:44:53–15:01:13	16:02:01–16:30:34	10.2 ± 0.2	21.6 ± 2.7	27.9 ± 0.4	148.2 ± 3.4
Na ⁺	Li _A	13:44:53–15:01:13	16:02:01–16:30:34	10.2 ± 0.2	17.7 ± 1.9	51.6 ± 1.1	249.0 ± 5.2
K ⁺	Li _A	13:44:53–15:01:13	16:02:01–16:30:34	10.2 ± 0.2	52.6 ± 2.7	56.6 ± 0.4	306.6 ± 3.2
NH ₄ ⁺	Li _A	13:44:53–15:01:13	16:02:01–16:30:34	10.2 ± 0.2	50.5 ± 2.3	57.4 ± 0.8	308.1 ± 4.2
Cl [−]	Li _B	13:44:53–15:01:13	16:02:01–16:30:34	10.2 ± 0.2	331.4 ± 1.8	−51.8 ± 0.3	137.6 ± 2.1
ClO ₄ [−]	Li _A	13:44:53–15:01:13	16:02:01–16:30:34	10.2 ± 0.2	327.6 ± 2.7	−59.5 ± 0.7	−29.6 ± 4.9

temperatures of $-57\text{ }^{\circ}\text{C}$ and $-69\text{ }^{\circ}\text{C}$ respectively, implying that liquid water could be present as concentrated brine at the Phoenix site, and many similar locations, for significant portions of the Martian summer. Soluble salts deduced from chemical divide modeling contain 1.3 wt.% water bound in them, which is a minimum limit on the total water associated with salts because insoluble hydrated salts could also be present and some salts may deliquesce to form brine. This minimum water content is consistent with minimum water contents between 1.5 to 3 wt.% water determined from orbital spectroscopy data and recent direct measurement by MSL.

ACKNOWLEDGEMENTS

Funding from NASA Mars Data Analysis grant # NNX10AN66G awarded to DCC. We would also like to thank two anonymous reviewers and Samuel Kounaves for their helpful comments.

APPENDIX A

Tables A.1 and A.2.

Table A.2

Values determined in our WCL data reduction and derived values for calculating final ion concentrations: the temperature over the analysis window (T), the calibration ISE slope corrected for temperature T (S_m), the ISE potential measured over the analysis window (E_s), the ionic strength (I), the ion activity (a), and the activity coefficient (γ). All concentrations are in mM, except for the pH.

	Analysis						
	T ($^{\circ}\text{C}$)	S_m (mV dec $^{-1}$)	E_s (mV)	I (m)	a (m)	γ	Conc. ^d (mM)
<i>Rosy Red</i>							
pH _a	8.4 ± 0.3	53.4 ± 0.4	-13.7 ± 0.9	0.017 ± 0.003	2.14E-8 ± 3.82E-9	-	7.67 ± 0.08
pH _b	-	-	-	-	-	-	-
pH _{irid}	8.8 ± 0.3	50.1 ± 0.4	223.3 ± 1.3	0.017 ± 0.003	5.06E-9 ± 9.28E-10	-	8.30 ± 0.08
Ca ²⁺	8.4 ± 0.3	27.8 ± 0.8	78.7 ± 0.0 ^b	0.017 ± 0.003	1.27E-4 ± 5.45E-5	0.62 ± 0.03	0.16 ± 0.07
Mg ²⁺	8.4 ± 0.3	27.4 ± 0.6	59.4 ± 1.1	0.017 ± 0.003	1.88E-3 ± 5.42E-4	0.64 ± 0.03	2.91 ± 0.85
Na ⁺	8.4 ± 0.3	51.1 ± 0.9	10.4 ± 0.7	0.017 ± 0.003	1.31E-3 ± 2.95E-4	0.88 ± 0.01	1.46 ± 0.33
K ⁺	8.4 ± 0.3	56.3 ± 0.6	-39.9 ± 0.7	0.017 ± 0.003	3.17E-4 ± 4.46E-5	0.88 ± 0.01	0.33 ± 0.05
NH ₄ ⁺	8.4 ± 0.3	56.9 ± 0.7	-43.7 ± 0.5	0.017 ± 0.003	4.31E-5 ± 7.5E-6 ^c	0.87 ± 0.01	0.02 ± 0.01
Cl ⁻	8.4 ± 0.3	-52.4 ± 0.3	313.7 ± 1.5	0.017 ± 0.003	5.09E-4 ± 4.72E-5	0.88 ± 0.01	0.39 ± 0.04
ClO ₄ ⁻	8.4 ± 0.3	-59.1 ± 0.7	75.8 ± 1.8	0.017 ± 0.003	2.54E-3 ± 4.69E-4	0.88 ± 0.01	2.89 ± 0.54
^a Cl ⁻	5.4 ± 0.3	-52.2 ± 0.3	251.6 ± 18.0	0.017 ± 0.003	7.64E-3 ± 6.08E-3	0.88 ± 0.01	8.73 ± 6.95
<i>Sorceress 1</i>							
pH _a	5.7 ± 1.2	56.1 ± 0.5	-6.5 ± 2.3	0.018 ± 0.004	4.80E-8 ± 8.90E-9	-	7.32 ± 0.08
pH _b	5.7 ± 1.2	56.5 ± 0.5	-13.7 ± 0.8	0.018 ± 0.004	4.01E-8 ± 6.99E-9	-	7.40 ± 0.08
pH _{irid}	5.7 ± 1.2	53.3 ± 0.4	246.7 ± 3.6	0.018 ± 0.004	1.01E-7 ± 2.72E-8	-	7.00 ± 0.12
Ca ²⁺	5.7 ± 1.2	27.3 ± 0.6	184.3 ± 2.5 ^b	0.018 ± 0.004	3.01E-4 ± 1.11E-4	0.61 ± 0.08	0.45 ± 0.18
Mg ²⁺	5.7 ± 1.2	26.6 ± 0.7	47.2 ± 0.6	0.018 ± 0.004	3.96E-3 ± 1.30E-3	0.63 ± 0.09	6.22 ± 2.23
Na ⁺	5.7 ± 1.2	50.0 ± 0.5	41.8 ± 1.1	0.018 ± 0.004	3.11E-3 ± 3.93E-4	0.88 ± 0.02	3.52 ± 0.45
K ⁺	5.7 ± 1.2	55.8 ± 1.4	6.5 ± 0.8	0.018 ± 0.004	4.67E-4 ± 1.57E-4	0.87 ± 0.02	0.50 ± 0.17
NH ₄ ⁺	5.7 ± 1.2	56.0 ± 1.0	-22.2 ± 2.0	0.018 ± 0.004	3.71E-6 ± 1.01E-6 ^c	0.87 ± 0.02	-0.03 ± 0.01
Cl ⁻	5.7 ± 1.2	-51.3 ± 0.3	314.2 ± 3.2	0.018 ± 0.004	8.60E-4 ± 1.48E-4	0.87 ± 0.02	0.79 ± 0.14
ClO ₄ ⁻	5.7 ± 1.2	-58.6 ± 0.7	72.2 ± 3.5	0.018 ± 0.004	1.85E-3 ± 4.34E-4	0.87 ± 0.02	2.11 ± 0.50
^a Cl ⁻	-	-	-	-	-	-	-
<i>Sorceress 2</i>							
pH _a	10.0 ± 0.1	55.8 ± 0.3	-96.8 ± 0.9	0.026 ± 0.008	3.01E-7 ± 3.81E-8	-	6.52 ± 0.05
pH _b	10.0 ± 0.1	53.5 ± 0.3	-63.8 ± 1.0	0.026 ± 0.008	1.39E-7 ± 2.72E-8	-	6.86 ± 0.08
pH _{irid}	10.0 ± 0.1	50.3 ± 0.4	135.7 ± 4.2	0.026 ± 0.008	1.60E-7 ± 4.87E-8	-	6.80 ± 0.13
Ca ²⁺	10.0 ± 0.1	27.9 ± 0.3	143.3 ± 2.2 ^b	0.026 ± 0.008	7.55E-5 ± 2.87E-5	0.57 ± 0.05	0.09 ± 0.04
Mg ²⁺	10.0 ± 0.1	27.9 ± 0.4	61.7 ± 0.6	0.026 ± 0.008	8.01E-4 ± 2.44E-4	0.60 ± 0.05	1.31 ± 0.41
Na ⁺	10.0 ± 0.1	51.5 ± 1.1	91.7 ± 0.5	0.026 ± 0.008	8.83E-4 ± 2.42E-4	0.86 ± 0.02	0.99 ± 0.27
K ⁺	10.0 ± 0.1	56.6 ± 0.4	93.6 ± 1.9	0.026 ± 0.008	1.71E-4 ± 2.75E-5	0.85 ± 0.02	0.17 ± 0.03
NH ₄ ⁺	10.0 ± 0.1	57.3 ± 0.8	62.2 ± 0.9	0.026 ± 0.008	2.59E-5 ± 5.61E-6 ^c	0.85 ± 0.02	0.00 ± 0.01
Cl ⁻	10.0 ± 0.1	-51.8 ± 0.3	315.2 ± 0.6	0.026 ± 0.008	3.73E-4 ± 3.97E-5	0.85 ± 0.02	0.24 ± 0.03
ClO ₄ ⁻	10.0 ± 0.1	-59.5 ± 0.7	127.1 ± 0.7	0.026 ± 0.008	2.33E-3 ± 4.70E-4	0.86 ± 0.02	2.72 ± 0.55
^a Cl ⁻	5.4 ± 0.3	-50.9 ± 2.8	242.6 ± 0.4	0.026 ± 0.008	8.71E-3 ± 2.45E-3	0.85 ± 0.02	10.19 ± 2.88

^a These Cl⁻ values were determined several sols after the initial analysis (sol 34 for Rosy Red and sol 116 for Sorceress 2) and correspond to the point at which SO₄²⁻ was completely titrated upon BaCl₂ addition, as indicated by a sharp increase in Ba²⁺ concentrations. SO₄²⁻ concentrations are calculated using the Cl⁻ concentrations at the end of BaCl₂ titration (Cl₂) and on the initial sol of analysis (Cl₁) as: SO₄²⁻ (mM) = (Cl₂ - Cl₁)/2.

^b Ca²⁺ ISE potentials have been corrected for ClO₄⁻ bias.

^c The calculated NH₄⁺ activity is corrected for interference from K⁺.

^d Final concentrations are corrected for ions already present in the calibration solution.

APPENDIX B

The graphs in this appendix show raw data and Kalman smoothed ISE potentials and temperatures on sol 30 of the Rosy Red WCL experiment. Gray data points are raw ISE potentials referenced to a Li⁺ ISE (or temperatures), and the red lines are the output from Kalman

smoothing. The addition of calibration salts and sample are indicated by vertical black dashed lines. Drawer open and close events are indicated by vertical gray dashed lines. The intervals used for calibration and analysis, corresponding to the analysis presented in Table 3, are given by black dots. [Figs. B.1–B.11.](#)

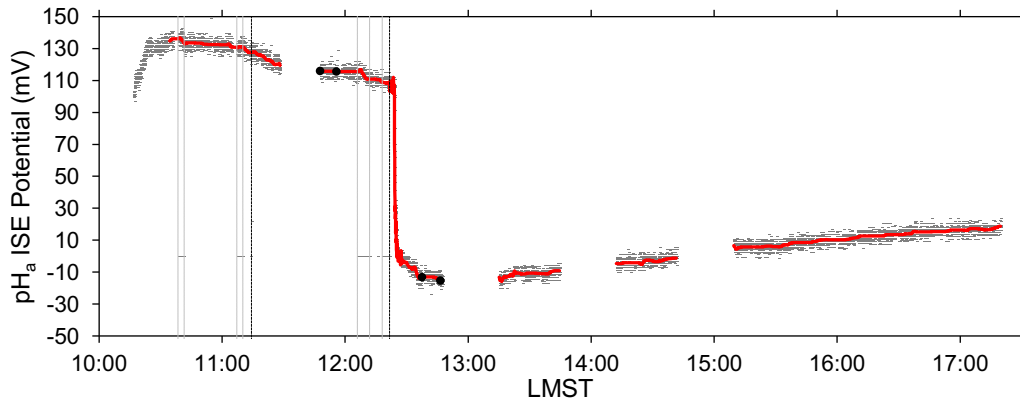


Fig. B.1. Rosy Red pH_a ISE potentials on sol 30.

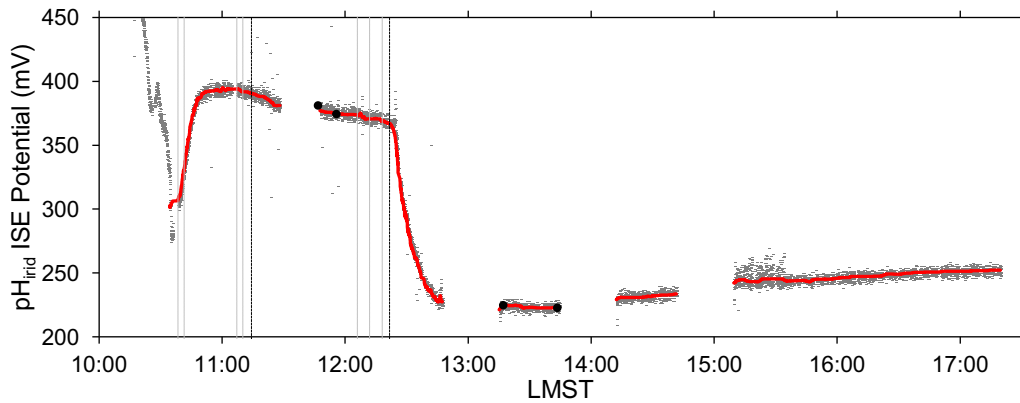


Fig. B.2. Rosy Red pH_{liquid} ISE potentials on sol 30.

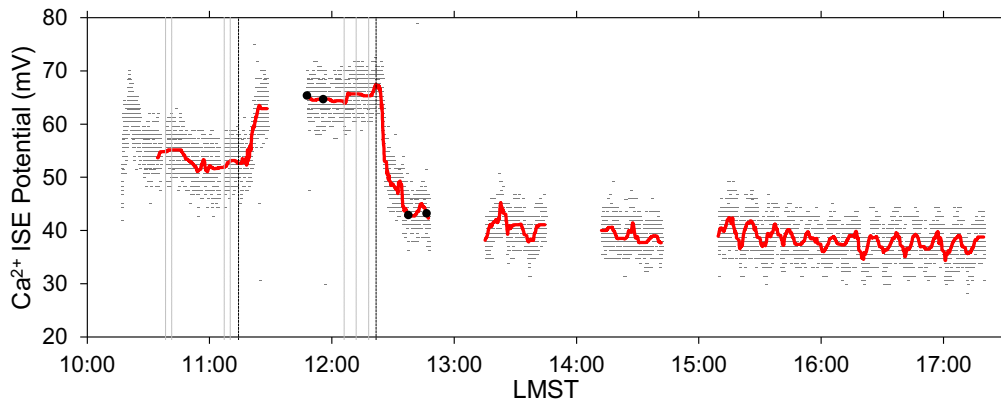
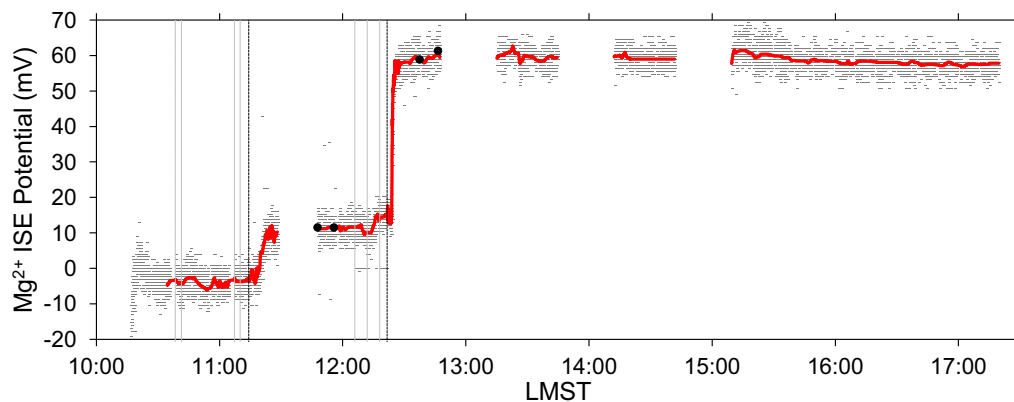
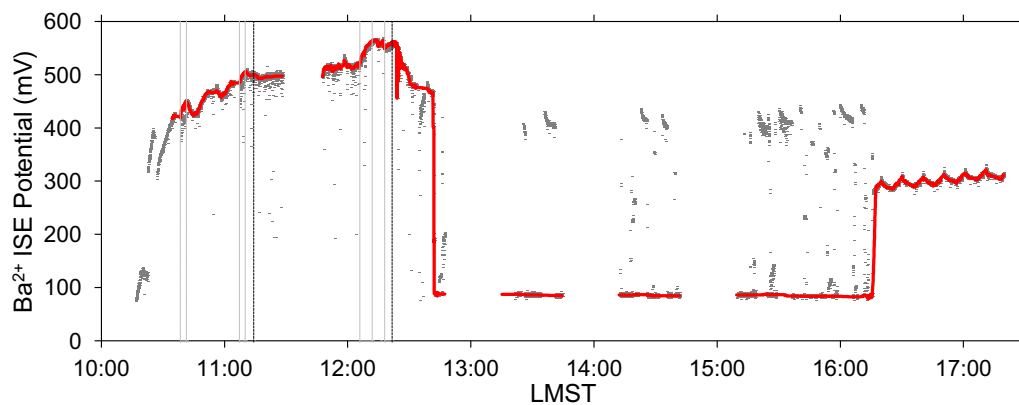
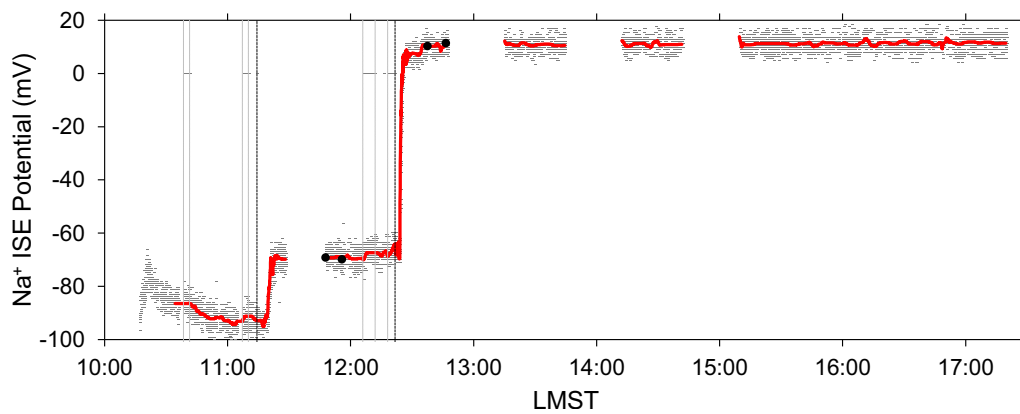
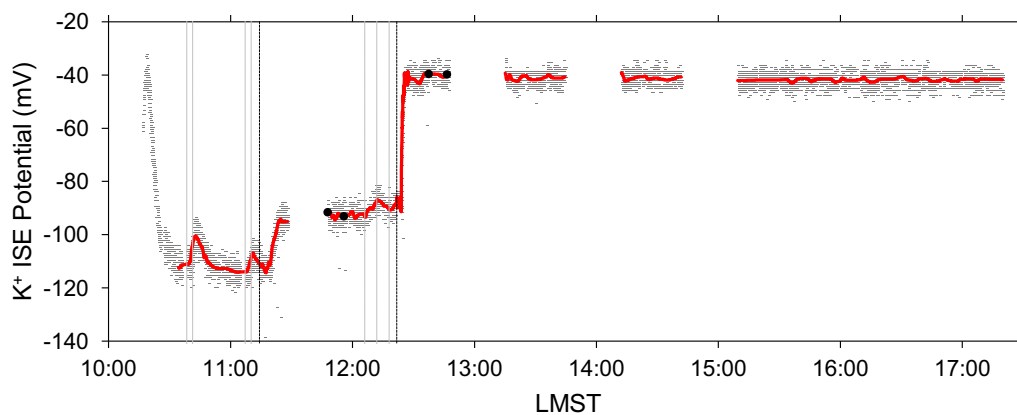
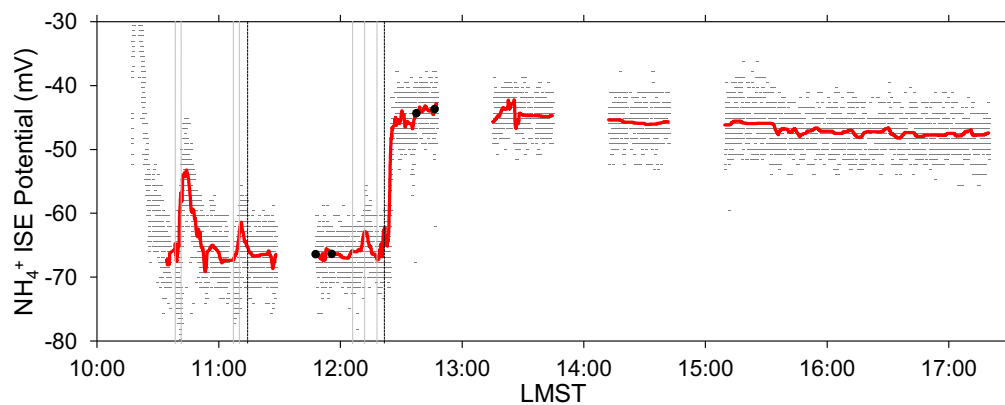
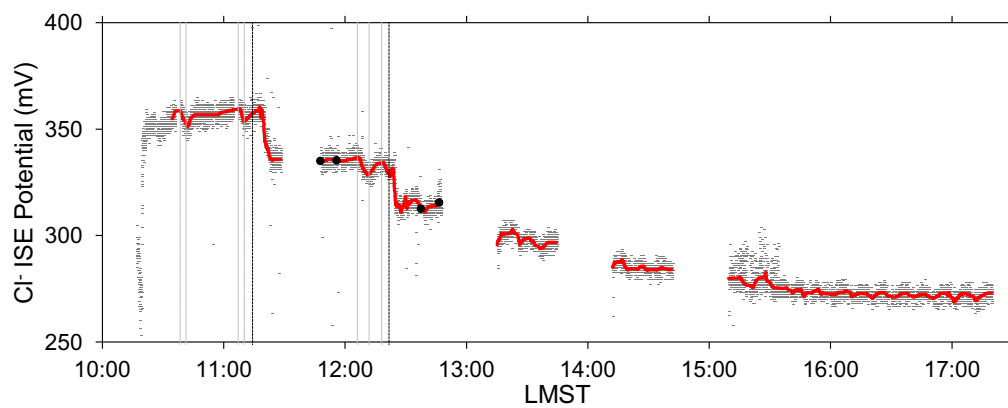


Fig. B.3. Rosy Red Ca²⁺ ISE potentials on sol 30.

Fig. B.4. Rosy Red Mg²⁺ ISE potentials on sol 30.Fig. B.5. Rosy Red Ba²⁺ ISE potentials on sol 30.Fig. B.6. Rosy Red Na⁺ ISE potentials on sol 30.

Fig. B.7. Rosy Red K⁺ ISE potentials on sol 30.Fig. B.8. Rosy Red NH₄⁺ ISE potentials on sol 30.Fig. B.9. Rosy Red Cl⁻ ISE potentials on sol 30.

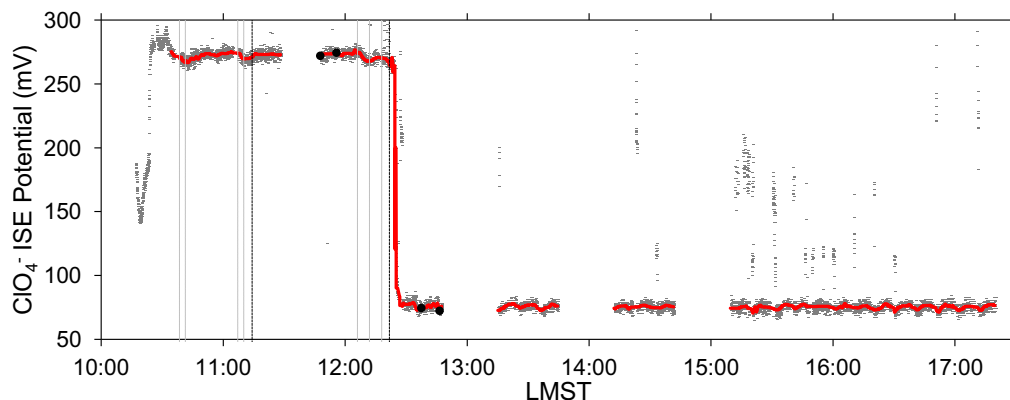
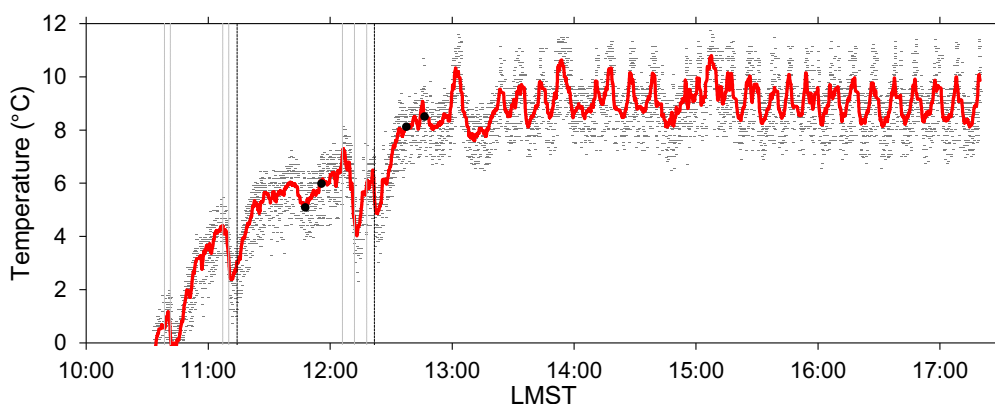
Fig. B.10. Rosy Red ClO_4^- ISE potentials on sol 30.

Fig. B.11. Rosy Red temperatures on sol 30.

REFERENCES

- Altheide T. S., Chevrier V., Nicholson C. and Denson J. (2009) Experimental investigation of the stability and evaporation of sulfate and chloride brines on Mars. *Earth Planet. Sci. Lett.* **282**, 69–78.
- Arvidson R. E., Bonitz R. G., Robinson M. L., Carsten J. L., Volpe R. A., Trebi-Ollennu A., Mellon M. T., Chu P. C., Davis K. R., Wilson J. J., Shaw A. S., Greenberger R. N., Siebach K. L., Stein T. C., Cull S. C., Goetz W., Morris R. V., Ming D. W., Keller H. U., Lemmon M. T., Sizemore H. G. and Mehta M. (2009) Results from the Mars Phoenix Lander Robotic Arm experiment. *J. Geophys. Res. Planets* **114**.
- Bandfield J. L., Glotch T. D. and Christensen P. R. (2003) Spectroscopic identification of carbonate minerals in the martian dust. *Science* **301**, 1084–1087.
- Bassett H. and Taylor H. S. (1912) Calcium nitrate. Part I. The two-component system: calcium nitrate–water. Part II. The three-component system: calcium nitrate–nitric acid–water at 25°. *J. Chem. Soc. Trans.* **101**, 576–585.
- Beatty D. W., Clifford S. M., Borg L. E., Catling D. C., Craddock R. A., Des Marais D. J., Farmer J. D., Frey H. V., Haberle R. M., McKay C. P., Newsom H. E., Parker T. J., Segura T. and Tanaka K. L. (2005) Key science questions from the second conference on early Mars: geologic, hydrologic, and climatic evolution and the implications for life. *Astrobiology* **5**, 663–689.
- Besley L. M. and Bottomley G. A. (1969) The water vapour equilibria over magnesium perchlorate hydrates. *J. Chem. Thermodyn.* **1**, 13–19.
- Bibring J. P., Langevin Y., Mustard J. F., Poulet F., Arvidson R., Gendrin A., Gondet B., Mangold N., Pinet P., Forget F. and Team O. (2006) Global mineralogical and aqueous mars history derived from OMEGA/Mars express data. *Science* **312**, 400–404.
- Bish D. L., Blake D. F., Vaniman D. T., Chipera S. J., Morris R. V., Ming D. W., Treiman A. H., Sarrazin P., Morrison S. M., Downs R. T., Achilles C. N., Yen A. S., Bristow T. F., Crisp J. A., Morookian J. M., Farmer J. D., Rampe E. B., Stolper E. M., Spanovich N. and Team M. S. (2013) X-ray diffraction results from mars science laboratory: mineralogy of rocknest at gale crater. *Science* **341**.
- Blake D. F., Morris R. V., Kocurek G., Morrison S. M., Downs R. T., Bish D., Ming D. W., Edgett K. S., Rubin D., Goetz W., Madsen M. B., Sullivan R., Gellert R., Campbell I., Treiman A. H., McLennan S. M., Yen A. S., Grotzinger J., Vaniman D. T., Chipera S. J., Achilles C. N., Rampe E. B., Sumner D., Meslin P. Y., Maurice S., Forni O., Gasnault O., Fisk M., Schmidt M., Mahaffy P., Leshin L. A., Glavin D., Steele A., Freissinet C., Navarro-González R., Yingst R. A., Kah L. C., Bridges N., Lewis K. W., Bristow T. F., Farmer J. D., Crisp J. A., Stolper E. M., DesMarais D. J. and Sarrazin P. (2013) Curiosity at gale crater, Mars: characterization and analysis of the rocknest sand shadow. *Science* **341**.

- Boynton W. V., Ming D. W., Kounaves S. P., Young S. M. M., Arvidson R. E., Hecht M. H., Hoffman J., Niles P. B., Hamara D. K., Quinn R. C., Smith P. H., Sutter B., Catling D. C. and Morris R. V. (2009) Evidence for calcium carbonate at the Mars Phoenix Landing Site. *Science* **325**, 61–64.
- Boynton W. V., Taylor G. J., Evans L. G., Reedy R. C., Starr R., Janes D. M., Kerry K. E., Drake D. M., Kim K. J., Williams R. M. S., Crombie M. K., Dohm J. M., Baker V., Metzger A. E., Karunatillake S., Keller J. M., Newsom H. E., Arnold J. R., Bruckner J., Englert P. A. J., Gasnault O., Sprague A. L., Mitrofanov I., Squyres S. W., Trombka J. I., d'Uston L., Wanke H. and Hamara D. K. (2007) Concentration of H, Si, Cl, K, Fe, and Th in the low- and mid-latitude regions of Mars. *J. Geophys. Res. Planet* **112**.
- Brass G. W. (1980) Stability of brines on Mars. *Icarus* **41**, 20–28.
- Brown S. D. (1986) The Kalman filter in analytical-chemistry. *Anal. Chim. Acta* **181**, 1–29.
- Chevrier V., Hanley J. and Altheide T. S. (2009) Stability of perchlorate hydrates and their liquid solutions at the Phoenix landing site. *Mars. Geophys. Res. Lett.* **36**.
- Clark B. C. (1978) Implications of abundant hygroscopic minerals in the Martian regolith. *Icarus* **34**, 645–665.
- Clark B. C., Baird A. K., Weldon R. J., Tsusaki D. M., Schnabel L. and Candelaria M. P. (1982) Chemical composition of Martian fines. *J. Geophys. Res.* **87**, 59–67.
- Coates J. D. and Achenbach L. A. (2004) Microbial perchlorate reduction: rocket-fuelled metabolism. *Nat. Rev. Microbiol.* **2**, 569–580.
- Cull S. C., Arvidson R. E., Catalano J. G., Ming D. W., Morris R. V., Mellon M. T. and Lemmon M. (2010) Concentrated perchlorate at the Mars Phoenix landing site: evidence for thin film liquid water on Mars. *Geophys. Res. Lett.* **37**.
- Davila A. F., Duport L. G., Melchiorri R., Jänchen J., Valea S., Rios A., Fairén A. G., Möhlmann D., McKay C. P., Ascaso C. and Wierchos J. (2010) Hygroscopic salts and the potential for life on Mars. *Astrobiology* **10**, 617–628.
- Dickinson W. W. and Rosen M. R. (2003) Antarctic permafrost: an analogue for water and diagenetic minerals on Mars. *Geology* **31**, 199–202.
- Dobrynina T. A., Chernyshova A. M., Akhapkina N. A. and Rosolovskii V. Y. (1980) Fusion diagram of the magnesium perchlorate–water system. *Russ. J. Inorg. Chem.* **25**, 2233–2236.
- Drever J. I. (1982) *The Geochemistry of Natural Waters*. Prentice-Hall, Englewood Cliffs, NJ.
- Ehlmann B. L., Mustard J. F., Murchie S. L., Poulet F., Bishop J. L., Brown A. J., Calvin W. M., Clark R. N., Des Marais D. J., Milliken R. E., Roach L. H., Roush T. L., Swayze G. A. and Wray J. J. (2008) Orbital identification of carbonate-bearing rocks on Mars. *Science* **322**, 1828–1832.
- Eugster H. P. and Jones B. F. (1979) Behavior of major solutes during closed-basin brine evolution. *Am. J. Sci.* **279**, 609–631.
- Ewjing W. W., Brandner J. D., Slichter C. B. and Griesinger W. K. (1933) The temperature-composition relations of the binary system magnesium nitrate–water. *J. Am. Chem. Soc.* **55**, 4822–4824.
- Fairén A. G., Davila A. F., Gago-Duport L., Amils R. and McKay C. P. (2009) Stability against freezing of aqueous solutions on early Mars. *Nature* **459**, 401–404.
- Feldman W. C., Mellon M. T., Maurice S., Prettyman T. H., Carey J. W., Vaniman D. T., Bish D. L., Fialips C. I., Chipera S. J., Kargel J. S., Elphic R. C., Funsten H. O., Lawrence D. J. and Tokar R. L. (2004a) Hydrated states of MgSO₄ at equatorial latitudes on Mars. *Geophys. Res. Lett.* **31**.
- Feldman W. C., Prettyman T. H., Maurice S., Plaut J. J., Bish D. L., Vaniman D. T., Mellon M. T., Metzger A. E., Squyres S. W., Karunatillake S., Boynton W. V., Elphic R. C., Funsten H. O., Lawrence D. J. and Tokar R. L. (2004b) Global distribution of near-surface hydrogen on Mars. *J. Geophys. Res. Planet* **109**, E09006.
- Fisher D. A., Hecht M. H., Kounaves S. P. and Catling D. C. (2010) A perchlorate brine lubricated deformable bed facilitating flow of the north polar cap of Mars: possible mechanism for water table recharging. *J. Geophys. Res. Planet* **115**, E00E12.
- Fritz S. J. (1994) A survey of charge-balance errors on published analyses of potable ground and surface waters. *Groundwater* **32**, 539–546.
- Gendrin, A., Bibring, J. P., Gondet, B., Langevin, Y., Mangold, N., Mustard, J. F., Poulet, F., and Quantin, C. (2004) Identification of sulfate deposits on Mars by OMEGA/Mars Express. In *Second Conference on Early Mars*, #8030 (abstr.).
- Gitterman K. E. (1937). In *Thermal analysis of sea water* (ed. CRREL TL). USA Cold Regions Research and Engineering Laboratory, Hanover, NH.
- Glotch T. D., Osterloo M. M., Hamilton V. E., Bandfield J. L., Baldridge A. M., Christensen P. R., Tornabene L. L., Anderson F. S., Che C. and Seelos F. P. (2008) Analysis of chloride salt deposits on Mars. *Geochim. Cosmochim. Acta* **72**, A314.
- Gough R. V., Chevrier V. F., Baustian K. J., Wise M. E. and Tolbert M. A. (2011) Laboratory studies of perchlorate phase transitions: Support for metastable aqueous perchlorate solutions on Mars. *Earth Planet. Sci. Lett.* **312**, 371–377.
- Grunthaner P., Hecht M. H., Tamppari L. and Smith P. (2009) *Phoenix Project MECA Wet Chemistry Laboratory Calibration Report*. Jet Propulsion Laboratory, California Institute of Technology.
- Hagedorn B., Sletten R. S., Hallet B., McTigue D. F. and Steig E. J. (2010) Ground ice recharge via brine transport in frozen soils of Victoria Valley, Antarctica: Insights from modeling $\delta^{18}\text{O}$ and δD profiles. *Geochim. Cosmochim. Acta* **74**, 435–448.
- Hanley J., Chevrier V. F., Berget D. J. and Adams R. D. (2012) Chlorate salts and solutions on Mars. *Geophys. Res. Lett.* **39**.
- Hardie L. H. and Eugster H. P. (1970) The evolution of closed-basin brines. *Mineral. Soc. Am. Special Paper* **3**, 273–290.
- Haskin L. A., Wang A., Jolliff B. L., McSween H. Y., Clark B. C., Des Marais D. J., McLennan S. M., Tosca N. J., Hurowitz J. A., Farmer J. D., Yen A., Squyres S. W., Arvidson R. E., Klingelhofer G., Schroder C., de Souza P. A., Ming D. W., Gellert R., Zipfel J., Bruckner J., Bell J. F., Herkenhoff K., Christensen P. R., Ruff S., Blaney D., Gorevan S., Cabrol N. A., Crumpler L., Grant J. and Soderblom L. (2005) Water alteration of rocks and soils on Mars at the Spirit rover site in Gusev crater. *Nature* **436**, 66–69.
- Hecht M. H., Kounaves S. P., Quinn R. C., West S. J., Young M. M., Ming D. W., Catling D. C., Clark B. C., Boynton W. V., Hoffman J., DeFlores L. P., Gospodinova K., Kapit J. and Smith P. H. (2009) Detection of Perchlorate and the Soluble Chemistry of Martian Soil at the Phoenix Lander Site. *Science* **325**, 64–67.
- Heet T. L., Arvidson R. E., Cull S. C., Mellon M. T. and Seelos K. D. (2009) Geomorphic and geologic settings of the Phoenix Lander mission landing site. *J. Geophys. Res. Planets* **114**.
- Helske, J., 2010. KFAS: Kalman Filter and Smoothers for Exponential Family State Space Models, R package version 0.9.11.
- Herut B., Starinsky A., Katz A. and Bein A. (1990) The role of seawater freezing in the formation of subsurface brines. *Geochim. Cosmochim. Acta* **54**, 13–21.
- Hurowitz J. A., McLennan S. M., Tosca N. J., Arvidson R. E., Michalski J. R., Ming D. W., Schroder C. and Squyres S. W. (2006) In situ and experimental evidence for acidic weathering of rocks and soils on Mars. *J. Geophys. Res. Planets* **111**.

- Johnson J. R., Bell J. F., Cloutis E., Staid M., Farrand W. H., McCoy T., Rice M., Wang A. and Yen A. (2007) Mineralogic constraints on sulfur-rich soils from Pancam spectra at Gusev crater, Mars. *Geophys. Res. Lett.* **34**.
- Kahn R. (1985) The evolution of CO₂ on Mars. *Icarus* **62**, 175–190.
- King P. L., Lescinsky D. T. and Nesbitt H. W. (2004) The composition and evolution of primordial solutions on Mars, with application to other planetary bodies. *Geochim. Cosmochim. Acta* **68**, 4993–5008.
- Kounaves S. P., Carriera G. D., O'Neil G. D., Stroble S. T. and Claire M. W. (2014) Evidence of martian perchlorate, chlorate, and nitrate in Mars meteorite EETA79001: implications for oxidants and organics. *Icarus* **229**, 206–213.
- Kounaves S. P., Folds K. E., Hansen V. M., Weber A. W., Carrier B. L. and Chaniotakis N. A. (2012) *Identity of the Perchlorate Parent Salt(s) at the Phoenix Mars Landing Site Based on Reanalysis of the Calcium Sensor Response*. AGU, San Francisco, CA.
- Kounaves S. P., Hecht M. H., Kapit J., Gospodinova K., DeFlores L., Quinn R. C., Boynton W. V., Clark B. C., Catling D. C., Hredzak P., Ming D. W., Moore Q., Shusterman J., Stroble S., West S. J. and Young S. M. M. (2010a) Wet Chemistry experiments on the 2007 Phoenix Mars Scout Lander mission: data analysis and results. *J. Geophys. Res.* **115**.
- Kounaves S. P., Hecht M. H., Kapit J., Quinn R. C., Catling D. C., Clark B. C., Ming D. W., Gospodinova K., Hredzak P., McElhoney K. and Shusterman J. (2010b) Soluble sulfate in the martian soil at the Phoenix landing site. *Geophys. Res. Lett.* **37**.
- Kounaves S. P., Hecht M. H., West S. J., Morookian J., Young M. M., Quinn R. C., Grunthaner P., Wen X., Weiler M., Cable C. A., Fisher A., Gospodinova K., Kapit J., Stroble S., Hsu P., Clark B. C., Ming D. W. and Smith P. H. (2009) The MECA Wet Chemistry Laboratory on the 2007 Phoenix Mars Scout Lander. *J. Geophys. Res.* **114**.
- Kuz'min R. O. and Zabalueva E. V. (1998) On Salt Solutions in the Martian Cryolithosphere. *Sol. Syst. Res.* **32**, 187–197.
- Lane M. D., Bishop J. L., Dyar M. D., King P. L., Parente M. and Hyde B. C. (2008) Mineralogy of the Paso Robles soils on Mars. *Am. Mineral.* **95**, 728–739.
- Langevin Y., Poulet F., Bibring J. P. and Gondet B. (2005) Sulfates in the north polar region of Mars detected by OMEGA/Mars express. *Science* **307**, 1584–1586.
- Langmuir D. (1965) Stability of carbonates in the system MgO–CO₂–H₂O. *J. Geol.* **73**, 730–754.
- Langmuir D. (1997) *Aqueous Environmental Geochemistry*. Prentice Hall, Upper Saddle River, NJ.
- Lavagnini I., Pastore P. and Magno F. (1990) Comparison of the Kalman filter and dedicated algorithms for processing data for solution equilibria, noise smoothing, and calibration. *Analyt. Chim. Acta* **239**, 95–106.
- Lenferink H. J., Durham W. B., Stern L. A. and Pathare A. V. (2013) Weakening of ice by magnesium perchlorate hydrate. *Mars Polar Science V* **225**, 940–948.
- Leshin L. A., Mahaffy P. R., Webster C. R., Cabane M., Coll P., Conrad P. G., Archer P. D., Atreya S. K., Brunner A. E., Buch A., Eigenbrode J. L., Flesch G. J., Franz H. B., Freissinet C., Glavin D. P., McAdam A. C., Miller K. E., Ming D. W., Morris R. V., Navarro-González R., Niles P. B., Owen T., Pepin R. O., Squyres S. W., Steel A., Stern J. C., Summons R. E., Sumner D. Y., Sutter B., Szopa C., Teinturier S., Trainer M. G., Wray J. J., Grotzinger J. P. and Team M. S. (2013) Volatile, isotope, and organic analysis of martian fines with the Mars curiosity rover. *Science* **341**.
- Lukow S. R. and Kounaves S. P. (2005) Analysis of simulated Martian Regolith using an array of ion selective electrodes. *Electroanalysis* **17**, 1441–1449.
- Marion G. M., Catling D. C., Crowley J. K. and Kargel J. S. (2011) Modeling hot spring chemistries with applications to martian silica formation. *Icarus* **212**, 629–642.
- Marion G. M., Catling D. C. and Kargel J. S. (2003) Modeling aqueous ferrous iron chemistry at low temperatures with application to Mars. *Geochim. Cosmochim. Acta* **67**, 4251–4266.
- Marion G. M., Catling D. C. and Kargel J. S. (2009) Br/Cl partitioning in chloride minerals in the Burns formation on Mars. *Icarus* **200**, 436–445.
- Marion G. M., Catling D. C., Zahnle K. J. and Claire M. W. (2010) Modeling aqueous perchlorate chemistries with applications to Mars. *Icarus* **207**, 675–685.
- Marion G. M. and Farren R. E. (1999) Mineral solubilities in the Na–K–Mg–Ca–Cl–SO₄–H₂O system: a re-evaluation of the sulfate chemistry in the Spencer–Møller–Weare model. *Geochim. Cosmochim. Acta* **63**, 1305–1318.
- Marion G. M., Farren R. E. and Komrowski A. J. (1999) Alternative pathways for seawater freezing. *Cold Reg. Sci. Technol.* **29**, 259–266.
- McSween H. Y. and Keil K. (2000) Mixing relationships in the Martian regolith and the composition of globally homogeneous dust. *Geochim. Cosmochim. Acta* **64**, 2155–2166.
- Mellon M. T., Arvidson R. E., Sizemore H. G., Searls M. L., Blaney D. L., Cull S., Hecht M. H., Heet T. L., Keller H. U., Lemmon M. T., Markiewicz W. J., Ming D. W., Morris R. V., Pike W. T. and Zent A. P. (2009) Ground ice at the Phoenix Landing site: stability state and origin. *J. Geophys. Res.* **114**.
- Mellon M. T., Boynton W. V., Feldman W. C., Arvidson R. E., Titus T. N., Bandfield J. L., Putzig N. E. and Sizemore H. G. (2008) A prelanding assessment of the ice table depth and ground ice characteristics in Martian permafrost at the Phoenix landing site. *J. Geophys. Res. Planets* **113**.
- Ming D. W., Archer P. D., Glavin D. P., Eigenbrode J. L., Franz H. B., Sutter B., Brunner A. E., Stern J. C., Freissinet C., McAdam A. C., Mahaffy P. R., Cabane M., Coll P., Campbell J. L., Atreya S. K., Niles P. B., Bell J. F., Bish D. L., Brinckerhoff W. B., Buch A., Conrad P. G., Des Marais D. J., Ehlmann B. L., Fairén A. G., Farley K., Flesch G. J., Francois P., Gellert R., Grant J. A., Grotzinger J. P., Gupta S., Herkenhoff K. E., Hurowitz J. A., Leshin L. A., Lewis K. W., McLennan S. M., Miller K. E., Moersch J., Morris R. V., Navarro-González R., Pavlov A. A., Perrett G. M., Pradler I., Squyres S. W., Summons R. E., Steele A., Stolper E. M., Sumner D. Y., Szopa C., Teinturier S., Trainer M. G., Treiman A. H., Vaniman D. T., Vasavada A. R., Webster C. R., Wray J. J. and Yingst R. A. (2013) Volatile and organic compositions of sedimentary rocks in yellowknife bay, gale crater, Mars. *Science*.
- Morris R. V., Ruff S. W., Gellert R., Ming D. W., Arvidson R. E., Clark B. C., Golden D. C., Siebach K., Klingelhofer G., Schroder C., Fleischer I., Yen A. S. and Squyres S. W. (2010) Identification of carbonate-rich outcrops on Mars by the Spirit Rover. *Science* **329**, 421–424.
- Murchie S. L., Mustard J. F., Ehlmann B. L., Milliken R. E., Bishop J. L., McKeown N. K., Dobrea E. Z. N., Seelos F. P., Buczkowski D. L., Wiseman S. M., Arvidson R. E., Wray J. J., Swayze G., Clark R. N., Marais D. J. D., McEwen A. S. and Bibring J. P. (2009) A synthesis of Martian aqueous mineralogy after 1 Mars year of observations from the Mars Reconnaissance Orbiter. *J. Geophys. Res. Planet* **114**, E00D06. <http://dx.doi.org/10.1029/2009JE003342>.
- Navarro-González R., Vargas E., de la Rosa J., Raga A. and McKay C. (2010) Reanalysis of the Viking results suggests perchlorate and organics at midlatitudes on Mars. *J. Geophys. Res. Planets* **115**.

- Nelson K. H. and Thompson T. G. (1954) *Deposition of Salts from Sea Water by Frigid Concentration*. University of Washington Dept. of Oceanography, Seattle, WA.
- Nelson M. J., Newsom H. E. and Draper D. S. (2005) Incipient hydrothermal alteration of basalts and the origin of Martian soil. *Geochim. Cosmochim. Acta* **69**, 2701–2711.
- Niles P. B., Catling D. C., Berger G., Chassefière E., Ehlmann B. L., Michalski J. R., Morris R. V., Ruff S. W. and Sutter B. (2013) Geochemistry of carbonates on Mars: implications for climate history and nature of aqueous environments. *Space Sci. Rev.* **174**, 301–328.
- Onoda G. Y. and De Bruyn P. L. (1966) Proton adsorption at the ferric oxide/aqueous solution interface: I. A kinetic study of adsorption. *Surf. Sci.* **1**, 48–63.
- Osterloo M. M., Anderson F. S., Hamilton V. E. and Hynek B. M. (2010) Geologic context of proposed chloride-bearing materials on Mars. *J. Geophys. Res. Planet* **115**.
- Osterloo M. M., Hamilton V. E., Bandfield J. L., Glotch T. D., Baldrige A. M., Christensen P. R., Tornabene L. L. and Anderson F. S. (2008) Chloride-bearing materials in the southern highlands of Mars. *Science* **319**, 1651–1654.
- Parkhurst, D. L., Appelo, C. A. J. (1999) User's guide to PHREEQC (version 2) – a computer program for speciation, reaction-path, 1D-transport, and inverse geochemical calculations, pp. 99–4259.
- Pestova O. N., Myund L. A., Khripun M. K. and Prigaro A. V. (2005) Polythermal study of the systems $M(\text{ClO}_4)_2\text{-H}_2\text{O}$ ($M^{2+} = \text{Mg}^{2+}, \text{Ca}^{2+}, \text{Sr}^{2+}, \text{Ba}^{2+}$). *Russ. J. Appl. Chem.* **78**, 409–413.
- Pitzer K. S. (1991) *Ion interaction approach: Theory and data correlation, Activity coefficients in Electrolyte Solutions*, second ed. CRC Press, Boca Raton, pp. 75–153.
- Quinn R. C., Chittenden J. D., Kounaves S. P. and Hecht M. H. (2011) The oxidation-reduction potential of aqueous soil solutions at the Mars Phoenix landing site. *Geophys. Res. Lett.* **38**.
- Quinn R. C. and Orenberg J. (1993) Simulations of the viking gas-exchange experiment using palagonite and fe-rich montmorillonite as terrestrial analogs – implications for the surface-composition of Mars. *Geochim. Cosmochim. Acta* **57**, 4611–4618.
- Rao B., Hatzinger P. B., Bohlke J. K., Sturchio N. C., Andrask B. J., Eckardt F. D. and Jackson W. A. (2010) Natural chlorate in the environment: application of a new IC-ESI/MS/MS method with a $\text{Cl}^{18}\text{O}_3^-$ internal standard. *Environ. Sci. Technol.* **44**, 8429–8434.
- Rennó N. O., Bos B. J., Catling D. C., Clark B. C., Drube L., Fisher D., Goetz W., Hviid S. F., Keller H. U., Kok J. F., Kounaves S. P., Leer K., Lemmon M. T., Madsen M. B., Markiewicz W. J., Marshall J., McKay C., Mehta M., Smith M., Zorzano M. P., Smith P. H., Stoker C. and Young S. M. M. (2009) Possible physical and thermodynamical evidence for liquid water at the Phoenix landing site. *J. Geophys. Res.* **114**.
- Ruesch O., Poulet F., Vincendon M., Bibring J. P., Carter J., Erkeling G., Gondet B. H. H., Ody A. and Reiss D. (2012) Compositional investigation of the proposed chloride-bearing materials on Mars using near-infrared orbital data from OMEGA/MEx. *J. Geophys. Res.* **117**.
- Rutan S. C. (1991) Adaptive Kalman filtering. *Anal. Chem.* **63**, 1103A–1109A.
- Sears D. W. G. and Chittenden J. D. (2005) On laboratory simulation and the temperature dependence of evaporation rate of brine on Mars. *Geophys. Res. Lett.* **32**.
- Silvester L. F. and Pitzer K. S. (1978) Thermodynamics of electrolytes. X. Enthalpy and the effect of temperature on the activity coefficients. *J. Solution Chem.* **7**, 327–337.
- Simon D. (2006) *Optimal State Estimation: Kalman, H-infinity and Nonlinear Approaches*, Wiley, Hoboken, NJ.
- Smith P. H., Tamppari L. K., Arvidson R. E., Bass D., Blaney D., Boynton W. V., Carswell A., Catling D. C., Clark B. C., Duck T., DeJong E., Fisher D., Goetz W., Gunnlaugsson H. P., Hecht M. H., Hipkin V., Hoffman J., Hviid S. F., Keller H. U., Kounaves S. P., Lange C. F., Lemmon M. T., Madsen M. B., Markiewicz W. J., Marshall J., McKay C. P., Mellon M. T., Ming D. W., Morris R. V., Pike W. T., Renno N., Staufer U., Stoker C., Taylor P., Whiteway J. A. and Zent A. P. (2009) H_2O at the Phoenix Landing Site. *Science* **325**, 58–61.
- Squyres S. W., Aharonson O., Arvidson R. E., Bell J. F., Christensen P. R., Clark B. C., Crisp J. A., Farrand W., Glotch T., Golombek M. P., Grant J., Grotzinger J., Herkenhoff K. E., Johnson J. R., Jolliff B. L., Knoll A. H., McLennan S. M., McSween H. Y., Moore J. M., Rice J. W. and Tosca N. (2006) Bedrock formation at Meridiani Planum. *Nature* **443**, E1–E2.
- Squyres S. W., Grotzinger J. P., Arvidson R. E., Bell J. F., Calvin W., Christensen P. R., Clark B. C., Crisp J. A., Farrand W. H., Herkenhoff K. E., Johnson J. R., Klingelhofer G., Knoll A. H., McLennan S. M., McSween H. Y., Morris R. V., Rice J. W., Rieder R. and Soderblom L. A. (2004) In situ evidence for an ancient aqueous environment at Meridiani Planum, Mars. *Science* **306**, 1709–1714.
- Steiger M., Linnow K., Ehrhardt D. and Rohde M. (2011) Decomposition reactions of magnesium sulfate hydrates and phase equilibria in the $\text{MgSO}_4\text{-H}_2\text{O}$ and $\text{Na}^+\text{-Mg}^{2+}\text{-Cl}^-\text{-SO}_4^{2-}\text{-H}_2\text{O}$ systems with implications for Mars. *Geochim. Cosmochim. Acta* **75**, 3600–3626.
- Stillman D. E. and Grimm R. E. (2011) Dielectric signatures of adsorbed and salty liquid water at the Phoenix landing site, Mars. *J. Geophys. Res.* **116**.
- Sutter B., Boynton W. V., Ming D. W., Niles P. B., Morris R. V., Golden D. C., Lauer H. V., Fellow C., Hamara D. K. and Mertzman S. A. (2012) The detection of carbonate in the martian soil at the Phoenix Landing site: A laboratory investigation and comparison with the Thermal and Evolved Gas Analyzer (TEGA) data. *Icarus* **218**, 290–296.
- Toner J. D., Catling D. C. and Bonnie L. (2014) The formation of supercooled brines, viscous liquids, and low temperature perchlorate glasses in aqueous solutions relevant to Mars. *Icarus* **233**, 36–47.
- Toner J. D. and Sletten R. S. (2013) The formation of Ca-Cl-rich groundwaters in the Dry Valleys of Antarctica: field measurements and modeling of reactive transport. *Geochim. Cosmochim. Acta* **110**, 84–105.
- Tosca N. J., Knoll A. H. and McLennan S. M. (2008) Water activity and the challenge for life on early Mars. *Science* **320**, 1204–1207.
- Tosca N. J. and McLennan S. M. (2006) Chemical divides and evaporite assemblages on Mars. *Earth Planet. Sci. Lett.* **241**, 21–31.
- Tusell F. (2011) Kalman filtering in R. *J. Stat. Softw.* **39**.
- Ugolini F. C. and Anderson D. M. (1973) Ionic migration and weathering in frozen Antarctic soils. *Soil Sci.* **115**, 461–470.
- Vaniman D. T., Bish D. L., Chipera S. J., Fialips C. I., Carey J. W. and Feldman W. C. (2004) Magnesium sulphate salts and the history of water on Mars. *Nature* **431**, 663–665.
- Wang A., Haskin L. A., Squyres S. W., Jolliff B. L., Crumpler L., Gellert R., Schroder C., Herkenhoff K., Hurowitz J., Tosca N. J., Farrand W. H., Anderson R. and Knudson A. T. (2006) Sulfate deposition in subsurface regolith in Gusev crater, Mars. *J. Geophys. Res. Planets* **111**.
- Yen A. S., Gellert R., Schroder C., Morris R. V., Bell J. F., Knudson A. T., Clark B. C., Ming D. W., Crisp J. A., Arvidson

R. E., Blaney D., Bruckner J., Christensen P. R., DesMarais D. J., de Souza P. A., Economou T. E., Ghosh A., Hahn B. C., Herkenhoff K. E., Haskin L. A., Hurowitz J. A., Joliff B. L., Johnson J. R., Klingelhofer G., Madsen M. B., McLennan S. M., McSween H. Y., Richter L., Rieder R., Rodionov D., Soderblom L., Squyres S. W., Tosca N. J., Wang A., Wyatt M. and Zipfel J. () An integrated view of the chemistry and mineralogy of martian soils. *Nature* **436**, 49–54.

Zorzano M. P., Marti E. M., Prieto-Ballesteros O., Osuna S. and Renno N. (2009) Stability of liquid saline water on present day Mars. *Geophys. Res. Lett.* **36**.

Associate editor: Penelope L. King